Power Factor Corrected High Gain Luo Converter Based Battery Charger for EV

A PROJECT REPORT

SUBMITTED IN PARTIAL FULFILLMENT OF THE REQUIREMENTS FOR THE AWARD OF THE DEGREE OF

MASTER OF TECHNOLOGY
IN
POWER ELECTRONICS AND SYSTEMS

Submitted by

Shalini Gupta

(2K20/PES/19)

Under the supervision of

Mr. Saurabh Mishra

Mr. Sikandar Ali Khan

DEPARTMENT OF ELECTRICAL ENGINEERING
DELHI TECHNOLOGICAL UNIVERSITY
(Formerly Delhi College of Engineering)
Bawana Road, Delhi-110042

May 2022

DEPARTMENT OF ELECTRICAL ENGINEERING
DELHI TECHNOLOGICAL UNIVERSITY
(Formerly Delhi College of Engineering)
Bawana Road, Delhi-110042

CANDIDATE'S DECLARATION

I, Shalini Gupta, Roll No –2K20/PES/19.student of M. Tech (Electrical Engineering), hereby declare that the project Dissertation titled "Power Factor Corrected High Gain Luo Converter Based Battery Charger for EV" which is submitted by us to the Electrical Engineering, Delhi Technological University, Delhi in partial fulfillment of the requirement for the award of the degree of Master of Technology, is original and not copied from any source without proper citation. This work has not previously formed the basis for the award of any Degree, Diploma Associateship, Fellowship or other similar title or recognition.

Place: Delhi Shalini Gupta

Date: 31.05.2022

DEPARTMENT OF ELECTRICAL ENGINEERING
DELHI TECHNOLOGICAL UNIVERSITY
(Formerly Delhi College of Engineering)
Bawana Road, Delhi-110042

CERTIFICATE

I hereby certify that the Project Dissertation titled "Power Factor Correction of High Gain Luo Converter Based Battery Charger for EV" which is submitted by Shalini Gupta, Roll No –2K20/pes/19. here, Electrical Engineering, Delhi Technological University, Delhi in partial fulfillment of the requirement for the award of the degree of Master of Technology, is a record of the project work carried out by the students under my supervision. To the best of my knowledge this work has not been submitted in part or full for any Degree or Diploma to this University or elsewhere.

SUPERVISOR
Mr. Saurabh

Mr. Sikandar Ali

Place: Delhi
Mishra

Khan

Date: 31.05.2022

ABSTRACT

One of the most important aspects to research and improve for Electric vehicles is batteries and chargers. Firstly, this thesis work deals with the lower system stresses for power factor correction at the front-end of an electric vehicle in a high step-up gain Luo converter, connected in series with a flyback converter for the battery charger. This deduction in switch voltage is produced in the conventional Luo converter by installing one switch and splitting the input inductor i.e., high gain Luo converter. While comparing the conventional Luo converter with the high gain Luo converter, for producing the same DC link voltage high gain Luo converter operates at a lower duty ratio due to the input switching inductor design. This is suitable for high-power EV chargers since the switching voltage and current stresses are massively decreased.

Secondly, this thesis work deals with the basic operation of the half-bridge LLC resonance converter for battery charging in resonant mode, step-down mode, and step-up mode. In this, we used the PI and PFM controller for producing the control frequency spectrum and for converting the control frequency signal into a pulse respectively. By comparing currents in resonance mode, the peak current of resonant current and magnetizing current is largely due to this primary side conduction losses increase in boost mode. In all three modes, the resonant mode provides excellent results. Finally, improvements have been implemented to boost efficiency and power factor. the power factor correction of LLC resonant DC-DC converter for battery charging of EVs. Under the load and supply voltage variations, steady-state topology is evaluated. For various supply voltage, power factor and THD% are computed, resulting in a low value of THD%. Due to this, we achieved a smooth sinusoidal supply current. In this, we determined that charging the battery near the resonance frequency is the best approach.

Mention all the converters have been simulated in MATLAB/SIMULINK based on the model and controlling algorithm.

DEPARTMENT OF ELECTRICAL ENGINEERING
DELHI TECHNOLOGICAL UNIVERSITY
(Formerly Delhi College of Engineering)
Bawana Road, Delhi-110042

ACKNOWLEDGEMENT

We wish to express our sincerest gratitude to Mr. Saurabh Mishra & Mr. Sikandar Ali Khan for his continuous guidance and mentorship that he provided us during the project. He showed us thepath to achieve our targets by explaining all the tasks to be done and explained to us the importance of this project as well as its industrial relevance. He was always ready to help us and clear our doubts regarding any hurdles in this project. Without his constant support and motivation, this project would not have been successful.

Place: Delhi Shalini Gupta

Date: 31.05.2022

CONTENT

LIST OF TABLES

LIST OF FIGURES

LIST OF SYMBOLS AND ABBREVIATION

V_o Output Voltage of DC-DC converter

V_{in} Input Voltage

D Duty Cycle

L_f Filter Inductance

C_f Filter Capacitance

$S_{1,2}$ Switches of High gain Luo Converter

C_o DC-Link Capacitance

L_o Output Inductance of High gain Luo converter

V_{oref} Reference Output Voltage

S_f Flyback Switch

D_f Flyback Diode

V_b Battery Voltage

I_b Battery Current

I_b* Reference Battery Current

V_G Gate Pulse

T Time Period

i_D Diode Current

P_i Input power

V_L Voltage across an inductor

V_s Voltage across a switch

I_s Supply current

L_m Magnetizing inductance

N_s Secondary side turn ratio

N_p Primary side turn ratio

λ Order of integration of FOPI

K_{cr} Critical constant

K_i Integral gain

K_p Proportional gain

T_{cr} Critical time constant

$Q_{1,2}$ Switch of LLC resonant converter

P_o Output Power

F_x Normalized switching frequency

f_r Series resonant frequency

f_p Prallel resonance frequency

Q Quality factor

R_{ac} Reflected load resistance

m Inductance ratio

L_m Magnetizing Inductor

I_m Magnetizing Current

L_r Resonant Inductance

C_r Resonant Capacitor

R_o Load Resistance

f_s Switching frequency

f_r Resonant frequency

n Turn ratio

Q Quality factor

V_{error} Error voltage

I_{s1} Switch current across switch 1

I_{Lr} Resonant current

f_{supply} Supply frequency

ΔV_d Voltage ripple of DC-link Capacitor

ΔI_L Current ripple of inductor

V_d Duty-link Voltage

V_d* Reference DC-link voltage

G_{pv} Proportional-Gain of voltage controller

G_{pi} Proportional-Gain of current controller

G_{ii} Integral-Gain of Current Controller

G_{pLLC} Proportional-Gain of LLC controller

G_{iLLC} Integral-Gain of LLC controller

CHAPTER 1

INTRODUCTION

1.1 HISTORY OF DC-DC CONVERTERS

The DC-DC conversion technique firstly invented in 1920. A potential divider or rheostat producing an output voltage less than the source voltage with ways of reducing performance is the easiest technique to convert the DC-DC voltage conversion. In addition, a multi-quadrant chopper is being designed for industrial and commercial applications using a DC-DC conversion technique (Rashid 2011). Communication technologically advanced at a breakneck pace, necessitating the development of lower-voltage DC supplies, resulting in the rapid expansion of DC-DC converter topologies. Choppers are powerful electrical circuits that transform fixed DC voltage magnitudes to variable DC voltage magnitudes. DC-DC converters are another name for DC choppers.

1.2 DEVELOPMENT OF LUO CONVERTERS

It is also known as Luo converters (LCs). In comparison to both primary and transformer type converters, it has the following advantages (Figure 1-1). Superb potential transformation gain, increased energy density, better efficiency, load potential, inductance current with minimal distortions, cheap technique with easy creation, and reduction of parasitic element causes are among the advantages.

1.2.1 First Generation Converters

Traditional converters are another name for these converters. It only runs in one quadrants and has a low power rating (approximately 100W).

Figure 1-1 Hierarchy chart of Luo converters

Fundamental converters

Fundamental converters (FCs) are categorized into three types based on their function: step-up, step-down, and buck-boost converters, according to Liu et al (1996) shown in (Figure1-1). The converter is called a buck converter when the voltage at the output side is smaller than the supply voltage. Buck-boost converters, also known as Cuk converters, provide an output voltage that is larger than or less than the supply voltage depending on the duty cycle. This converter's output voltage

polarity is the inverse of the input supply voltage. When the power switch is turned off, it saves the energy transmitted to the output and capacitance. The parasitic components, semiconductors switch, and rectifiers power diode all limit the load voltage and gain of the FCs (Lu et al 2003).

Transformer-type converters

Between the 1960s and the 1980s, transformer type converters (TTCs) were developed (Figure1.1). Isolating type converters, or TTCs, are DC-DC converters that contain isolation (built into the transformer) between the source and the load circuits. Again, there are six kinds of converters: forward converters, flyback converters, push-pull converters, half-bridge converters, bridge converters, and zeta converters. TTCs have a high voltage transfer gain when both the input and output sides are connected with high insulation. The turn ratio N of the transformer determines the gain of all these TTCs. The forward converter is an ON/OFF power source that delivers power to the transformers secondaries while the transistor is in closed state. Even though FC can be designed for a significant amount of Po, it is commonly used where Po is less than 200W. The limitations are caused by the power device's inability to handle voltage and current shocks.

The push-pull stage of the step-up converter totally removes the iron cores saturations. The PPC has two switch that function concurrently and provide twice the load voltage. Two forwards converter are stacked back - back and supply with the same Vin, with each one dividing power to the load half-cycle apart. A half-bridge converter is what it's called. As a result, an additional driver circuit is required. A classic step-up converter configuration is the SEPIC converter. All transformer-based DC-DC converters are designed to run at a high frequency.

The switch must be capable of considerable voltage blocking while working from a rectified AC source, which is a significant disadvantage of single switch topology. Skin and proximity effects induce an increase in transformer coil losses. The losses induced by harmonics increase coil power losses, resulting in a high frequency of transformer coils and a rise in operating heat.

Developed-type converters

The developed type converters (DTCs) have solved the concerns discussed in Fundamental Converters. The fundamental work was presented at a Massey &Snyder conference (1977). He also designed a low-pass filter for the three types of converter that are produced from FCs. In the 1970s and 1990s, this type of conversion

procedure was highly common. All of these DTCs have little output voltage ripple in general (it can be lower than 2 percent).

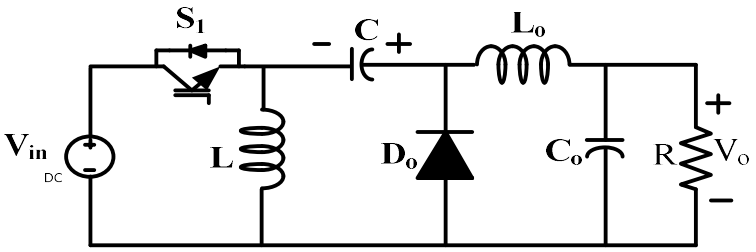

Figure 1-2 Power circuit diagram of POLC

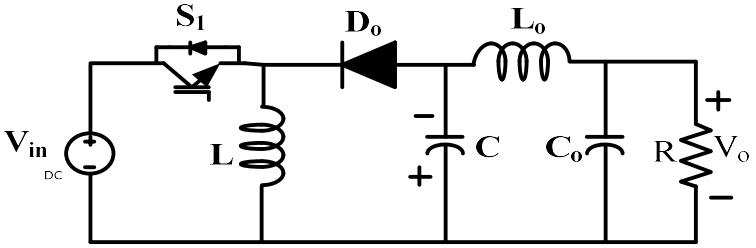

Figure 1-3 Power circuit diagram of NOLC

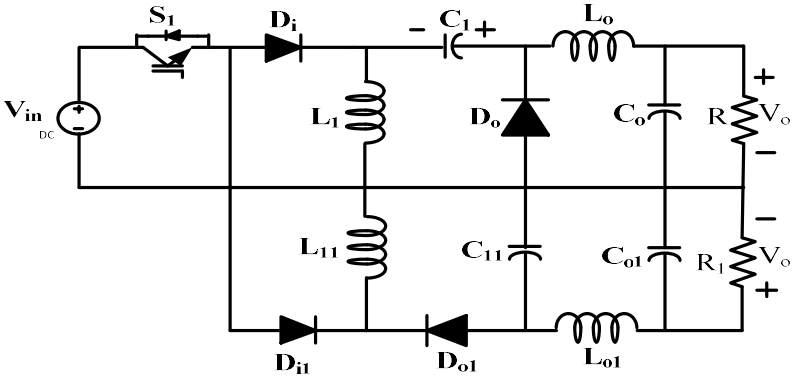

Figure 1-4 Power circuit diagram of DOLC

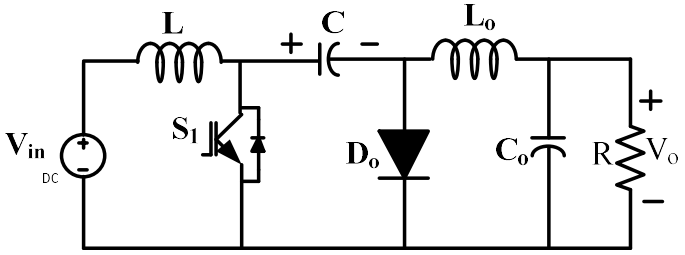

Figure 1-5 Power circuit diagram of Cuk converter

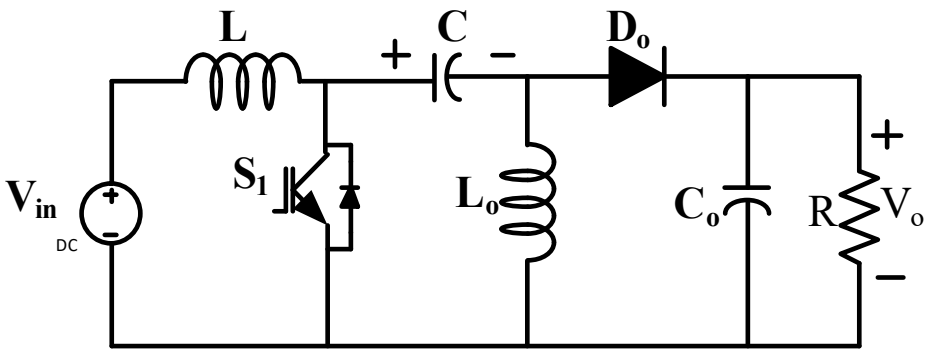

Figure 1-6 Power circuit diagram of SEPIC converter

Energizing takes happens exclusively in the turn-ON state of switch S1 in all of these converters. When switch S1 is turned off, the stored energy of its inductance and capacitance is relocated to the load and capacitors. As a result, all of these converters' output voltages are calculated using the calculation,

$$\frac{V_0}{V_{in}} = \frac{2D}{(1-D)}$$

The buck-boost converter is used to design the POLC, NOLC, and DOLC as shown in Figures 1-2, 1-3, and 1-4. In reality, the ripple on either the input or output sides can be eliminated by carefully adjusting the inductor values. The voltage magnitude can also be increased or decreased by the SEPIC. The boost converter is where it comes from.

Voltage-lift converters

The LC hierarchy chart is shown in Figures 1-7. The VLT, SLT, and ULT are the three main LC techniques. The voltage Lift Technique is a great strategy for raising the output voltage. This approach has been effectively implemented in the DC-DC conversion after years of industrial application and research.

The gain is raised in arithmetic series by Voltage Lift technique. It is divided into two types: positive and negative LCs. Elementary, Self-lifts, Re-lifts, and Multiple-lifts circuits can be found in VLT's positive and negative circuits (Figure 1.7). The self-lift circuit is built on top of the basic circuit. Two diodes, two capacitance, one

inductance, and one switch make up the re-lift circuit, which is derived from the self-lift circuit.

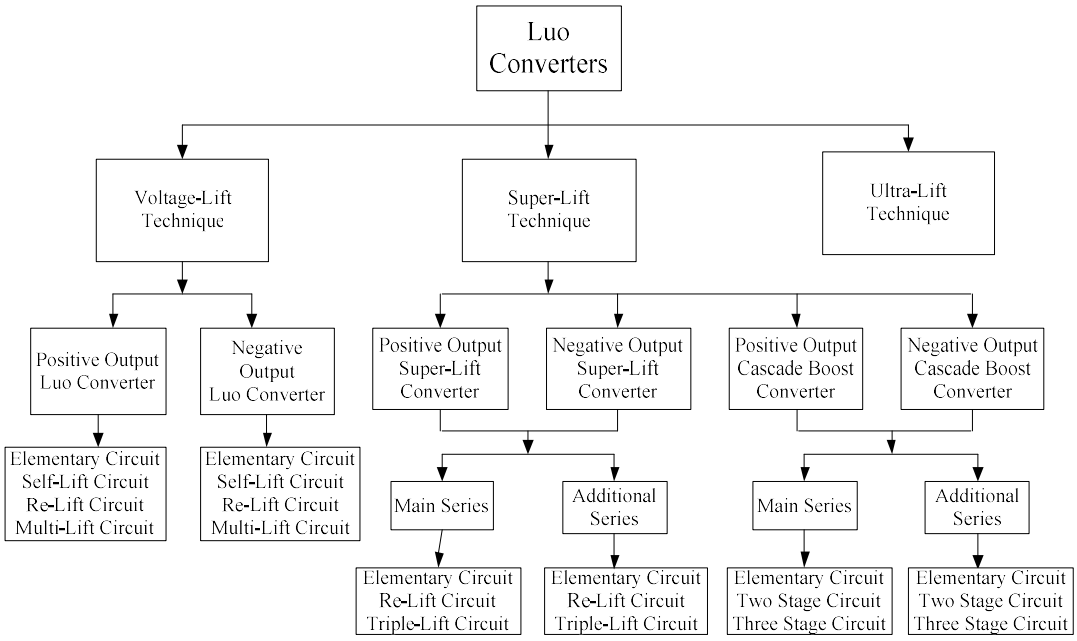

Figure 1-7 Hierarchy diagram of Luo-Converter based on lifting techniques

Super-lift converters

A novel method known as SLT has been developed, in which the output voltage increases in a geometric progression. As illustrated in Table 1.1.

Table 1.1 Comparison of various LC's voltage transfer gain

DC-DC Converter Topology (Elementary Circuit)	Voltage Transfer Gain	Duty Cycle (d)					
		0.2	0.33	0.5	0.67	0.8	0.9
Step-down	G =Vo/Vin=d	0.2	0.33	0.5	0.67	0.8	0.9
Step-up	G =Vo/Vin=1/1-d	1.25	1.5	2	3	5	10
Buck-Boost	G =Vo/Vin=d/1-d	0.25	0.5	1	2	4	9
Luo-Converters	G =Vo/Vin=n/1-d n-stage number	0.25	0.5	1	2	4	9
Super Lift-Luo Converters	G =Vo/Vin=2-d/1-d	2.25	2.5	3	4	6	11
Ultra Lift-Luo Converters	G =Vo/Vin=(2-d/1-d)-1	0.56	1.25	3	8	24	99

The main series triple-lift circuit employing SLT is created by attaching one inductor, three diodes, and two capacitance to the Re-lift circuits. The new series employing Super Lift Techniques is created by attaching merely two diodes and two capacitance to the primary series.

Ultra-lift converter

By comparing VLT and SLT, the ULT has created the highest voltage transfer gain. It combines the features of both the VLT and the SLT. Table 1.1 shows the comparison of the elementary circuit of several LC voltage-transfer gains.

1.2.2 Second Generation Converters

It has two-quadrants and four-quadrant operations, i.e. the averaging output power (100W or higher). Two major strategies will be used to classify the topologies. Initially, numerous quadrant choppers are used to design converters. The transformers are used to create the converters in the next category. For a long time, all of these converters were used for industrial applications.

1.2.3 Third Generation Converters

The switched component converter is another term for the 3rd generation converters. These types of converters are made up of inductance or capacitance and are hence called switched-inductor and capacitor converters. They have a wide range of output power and may operate in the second and fourth quadrants. As a result, the energy density and efficiency are high.

1.2.4 Fourth Generation Converters

Soft-switching converters are the fourth generation converters. Resonance switch converter, load-resonance converter, resonance-dc-link converter, and large-frequency-link integral-half-period converters are four typical soft-switching converter approaches. This resonance can be operated independently of the output using the switch approach. These converters have a wide range of output power and may operate in two and four quadrants (1000 W). As the transferred power increases, the power losses increase as well. Through the close and open states of the switch, significant losses are created. The key to enhancing power transfer capabilities is to reduce power losses across the switch. This problem has been solved thanks to the

gentle switching technique. Professor Fred Lee developed this approach, as well as established a research center, and provided support for the implementation of ZCS and ZVS-based DC-DC converters.

1.2.5 Fifth Generation Converters

For instance, power supplies with low output voltage and high current are used in the communication area, computer hardware, and many other applications. For PCs with Pentium I, II, III, and IV processors, the power supply range is 3.3 V, 2.5V, 1.8V, and 1.5V. The diode voltage loss is too great for a standard bridge diode rectifier to create such a low power supply voltage range. Novel varieties of MOSFETs are being developed for this purpose.

1.2.6 Sixth Generation Converters

Multiple power-storages element Resonance (MER) converters are the sixth generation converters. The main plants and equipment are current source resonant inverters. The SRC and PRC, which have two, three, or four power storing components, are the most common topologies depicted in the literature.

1.3 MODELING AND ANALYSIS OF DC-DC CONVERTER

In nonlinear dynamic plants, DC-DC converters are employed. Switching power devices and passive parts are the main sources of non-linearities. Non-rotate machinery, storages element, and parasitic element are common examples. Figure 1-8 depicts a hierarchy chart of DC-DC energy converter in continuous analysis. To demonstrate the low-frequency responsiveness of such plants, simple systematic relations in terms of circuit components were constructed.

Middle brook and Cuk (1977) introduced the SSAM for the classic DC-DC converter, which universalized the above-mentioned technique. The SSAM is a well-known tool for analyzing and constructing power converters. SSAM is a set of LTI state equations that describes the tiny signal performance of switching converters. The duty ratio of the switched converter drives each state equation, similar to variable structure control (VSC). By balancing the device matrix depending on the duty ratio, the averaged model is obtained. The averaging method's correctness is based on the assumption of low load ripple and the averaging output filter's corner frequency being substantially lower than the switching frequency.

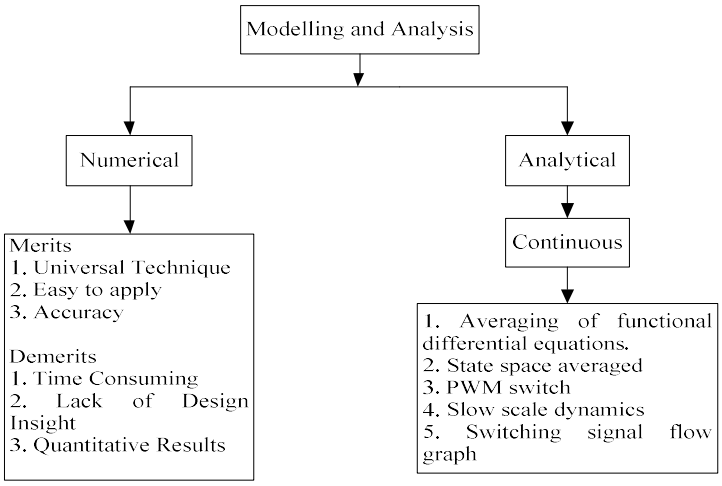

Figure 1-8 Hierarchy chart of various modelling family

This SFG approach has a simple design. However, because the method averages out the large frequency components, dynamic qualities are still limited. It makes the regulator unsuitable for large-signal dynamic control. SMC has been studied using a small-signal analysis of DC-DC converters. (Mattavelliet al 1997). SSAM was used for the modeling investigation of KY converters because of these factors.

1.4 Batteries and Battery Charging Technology for EVs

Despite the benefits of electric cars, technological limitations such as higher costs than equivalently sized gasoline engines, long charging periods [9]. The most important components to research and improve the barrier is the battery.

Lead-acid batteries, NiMH batteries, and Li-ion batteries are the three primary battery technologies now used in EVs, with their key attributes shown in Table 1-2 [14].

Table 1.2 The comparison of Batteries for electric vehicles [14]

Type	**Cost**	**Energy density**	**Discharge power capacity**	**Self-discharge rate**	**Life span**
Lead-acid	Affordable	Low	Good	High	Short
Ni-MH	High	High	Good	High	Long
Li-ion	Reasonable	High	Good	Low	Long

The following are some of the advantages [12, 22-25]:

1. One of the most appealing features is the higher power density. Li-ion battery has less weight than other types of battery when it comes to providing the same level of capacity.
2. Lithium-ion cells have a self-discharge rate of 2 - 3 percent, which is substantially less than Lead-Acid (4 - 6 percent) and Ni-MH (30 percent) per month. As a result, the Li-ion battery has a substantially longer life expectancy than other types of batteries. Furthermore, the Lithium-ion battery's discharge curve is flat. It is commonly understood that if the battery's power output drops rapidly during the discharging period, a dangerous issue can arise towards the end of the period, for high-energy applications. The Lithium-ion battery, as illustrated in Fig. 1-9, offers essentially constant voltages for about 80% of the discharge cycle.
3. The inside of a Lithium-ion battery pack has a high number of cells [26]. The 196 cells in the Nissan Leaf battery packs, for example, are made up of 48 modules, each with four cells [27, 28]. The charging process is faster and more efficient with this arrangement.

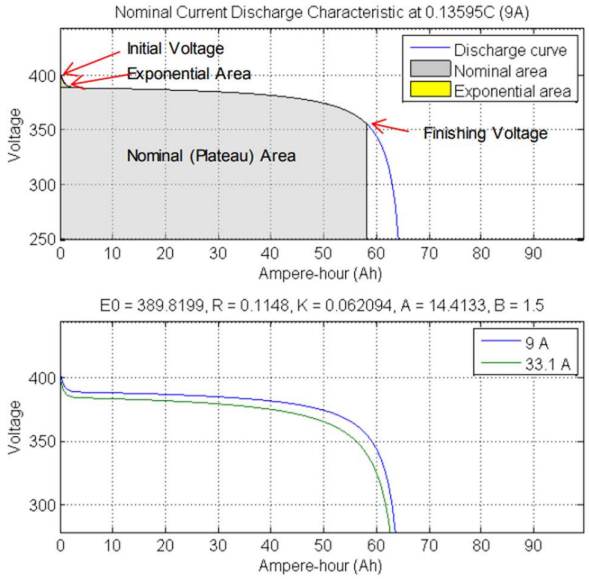

Fig.1-9 The Li-ion discharge characteristics

Battery charging technology

The charger and discharger, as well as the battery's design, have an impact on battery performance. Results, battery charging and discharging operations, and controlling are critical techniques in all-electric vehicle systems [29].

Charging strategy

Constant currents [30], constant voltages [31], constant power, taper current, and other charging methods exist [32]. The CV charger is the fundamental technology for the battery charger. It works by providing a suitable current to keep constant battery voltages. To protect the battery requires an additional circuit. A constant current charger feeds a fixed current into the battery (typically the max currents for a fast charger), and the battery voltages increase gradually w. r. t. time. When charging in homes, the key restriction is the max currents, which must be lower than the single-phase output fuse current.

Charging power levels

Based on various power levels and charger periods, battery chargers are divided into these categories:

Table 1.3 Comparison of charging power levels

Type	Classification	Voltage	Power level	Charging time
Level 1	Slow charging	120V @ AC	2 kW	10-12 Hours
Level 2	Primary charging	240V @ AC	19.2 kW	4 Hours
Level 3	DC fast charging	200V-800V @ DC	50kW- 120kW	Less than 1 hour

Level 1 charging is the most basic EV charger level. It is powered by a typical 120 V household socket and has a range of 4 to 5 miles after an hour of charging. Because most EV manufacturers include a Level 1 EV-SE wire set, no additional charger hardware is necessary. Recharging completely depleted EV batteries takes about 20 hours [3]. The use of a 220 V inventory framework is mostly limited to North, South, and Central America, Europe, and a big section of the world. This type of charging mechanism requires an installation cost of around 500-880 USD.

Level 2 charging tools use a private 230 V supplies system or a 208 V charging station outer [3]. In an hour of charging, a 3.3 KW onboard charger can provide roughly 15 miles of travel. A 6.6 KW onboard charging, on the other hand, may travel 30 miles in the same amount of time as it takes to charge. Level 2 EVSEs

employ equipment specifically designed to speed up recharging and require skilled electrical installation using a dedicated electrical line. The Level 2 charging system will cost between 1000 and 3000 dollars to set up.

A 480 V AC supply system is required for Level 3 charging. This kind of charger may travel 80 to 100 miles in 20 to 30 minutes after charging.

Off-board and on-board charger

When electric vehicles are hooked into a household utility socket overnight, onboard charging allows straightforward charging.

Table 1.4 Comparison of off-board and on-board charger

Classification	**Size limit**	**Weight limit**	**Space limit**	**Construction requirement**	**Power rating**	**Level type**	**Charging time**
Off-Board	less	Less	Less	Yes	50kW	3	Fast charging less than 1 hr
On-board	Yes	Yes	Yes	Less	2-20kW	1,2	Slow charging 4-12 hrs

1.7. Design requirement of EV battery charger

The research work primarily focuses on the onboard charger which typically consists of two stages, input-end PFC and dc-dc converters. The prime objective while designing an onboard charger is:

- The unity power factor for better power quality
- High efficiency
- Reduction in size and weight of the charger
- High power density
- Isolation at the output end for enhanced safety

1.8 OUTLINE

This thesis contains five chapters as follows:

Chapter 1: In this chapter, discussed the DC-DC converter is discussed, as well as several modeling methodologies for switched power converters. At the end of this chapter, the outline is clearly stated.

Chapter 2: In this chapter, the literature review of DC-DC converters, different types of control techniques, Electric Vehicles, Batteries and batteries Charging of EV, Onboard charger, Off-board charger, and Soft Switching and LLC resonant converter stated.

Chapter 3: In this chapter, a brief discussion on Power Factor Correction of High Gain Luo Converter Based EV Battery Charger. At the end of this chapter, it is suitable for high-power EV chargers since the switching voltage and current stresses are massively decreased.

Chapter 4: In this chapter, a brief discussion on half-bridge LLC resonant DC-DC converter for battery charging in all three modes i.e. resonant mode, buck mode, and boost mode. the pulse frequency modulation controller converts the control frequency signal into a pulse. In this we discussed power factor correction LLC resonant DC-DC converters for battery chargers of EV. Under the load and supply voltage variations, steady-state topology is evaluated. For various supply voltage, power factor, and THD% are computed in this chapter. We achieved a smooth sinusoidal supply current as we calculated that THD% is very low. In this, we determined that charging the battery near the resonance frequency is the best approach.

Chapter 5: In this chapter, we summarise all the chapters on onboard battery charging for electric vehicles, after that, there will be a future scope of study that will be continued to improve and develop battery chargers.

CHAPTER 2

LITERATURE SURVEY

2.1 DC-DC CONVERTER

As we discussed in chapter 1 DC-DC converters are categorized into 6 generations. In 1920,[1] created the basic structure circuits, which are made up of step-down, step-up, and Buck-Boost converters. The series of the produced converter was carried out by [2]. Cuk, Sepic, POLC, NOLC, and DOLC were created between 1970 and 1990. The voltage Lift (V.L) converter is the third type of converter. Self-Lift, re-lift, triple-lift, quadruple-lift, and high-stage-lift converters are five sub-series of this technology. During the years 2000 to 2003, [3] developed another approach known as the Super Lift (S.L) converters. POLC , NOLC, positive output cascaded step-up, and negative output cascaded step-up converters are the four types of Super Lift converters. A comparison of the VTG examined DC/DC converter under several duty cycles is presented by [4]. The voltage lift method was presented by [5]. In dc-dc converters, it's a popular method. The load voltage may be readily increased by 10 to 100 times using this approach. According to the amount of voltage lift circuits (VLC) utilized, VLC are classified as self-lift, re-lift, triple-lift, quadruple-lift, and high-stage lift converters. The configurations of the self-lift circuit and the re-lift circuit of series POLC were done by [6]. The self-lift and re-lift circuits of series positive output Luo converters have been explained by [7]. POSLL and PORLL converters are the abbreviations for such two circuits. Similarly, the negative output Luo converters' self-lift circuit is denoted as NOSLL converter. The output voltage gain of voltage lift and super lift Luo converters is described by [8]. These converters' output voltage rises in stages, following the arithmetic progression. As a result, an effective approach, the SL techniques, has been created, which may gradually raise the VTG in the geometric progression. [9] presented several dc-dc converters applications. Voltage lift and super lift methods, as well as Luo converters, have been employed by [10]. It has a high VTG, which is only the most sought-after characteristic in dc-dc converters.

2.2 CONTROL TECHNIQUES

The supply voltage feed-forwarding in open-loop controls has been studied by [11]. Input voltage feed-forward is proven to considerably reduce the effect of input voltage changes. [12] looked at a nonlinear PI controller that was constructed using advanced linearization theory. This is similar in structure to a fuzzy logic-based nonlinear PI controller. The benefits of certain fuzzy controllers over conventional PI controllers in controlling the Boost converter were described by [13]. Another fuzzy PI controller for the Cuk converter was presented by [14]. The fuzzy logic controller has been studied by [15]. In this, the resultant changes in the rate of the output voltages error are the fuzzy controller's inputs. The fuzzy controller determines the coefficient of the PI gains. Alternatively, the inaccuracy of both the load voltage and the supply inductance current might be used as the fuzzy base. Control structures are given importance by [16]. This is easy to regulate the load voltage to the specified value by indirectly managing the input inductor currents. With the ref voltage and load, the reference current may be determined. The study of sliding mode control proposed by [17] comprises an evaluation of these conditions: the reaching conditions, existence conditions, and characteristics in sliding modes. [18] investigated several slide surfaces for a simplified Ck converter with one, two, or three-state variables under ideal conditions. Only state variables, like supply inductance current, can govern dc-dc converter from an energy perspective, according to [19]. Only the inductor current was employed as the state variable in this sliding mode controller. [20] proposed that the sliding surface be implemented using the load voltage and its derivatives, the output capacitance current. [21] employed an HPF to acquire the resultant signal of the supply inductance current, whereas the results of the load voltage were calculated by subtracting the load voltage from the ref voltage. As a result, the ref current isn't required. The traditional two sliding mode control, according to [22], is comparable to the current modes control with Proportional Integral controller in the load voltage loops. As a result, a fuzzy-based control may be used to change the coefficients of the PI compensator.

2.3 Electric Vehicles

[23], [24] have presented EVs are driven by machines and are powered directly from sources of power rather than indirectly through an internal combustion engine. [25] have performed Electric Vehicles are more eco-friendly than traditional fossil fuels-

power vehicles, emitting less carbon dioxide, consuming less fuel, and emitting fewer pollutants. As a result, EVs are becoming the most popular across the world. Plug-in electric cars driven by power from a low carbon emissions grid, according to [26], can bring major benefits in terms of decreasing the climatic effect of transportation and reducing the transportation grid's dependency on oil-dependent fuel. PEVs minimize running expenses while also providing a cleaner and quieter atmosphere. Uncoordinated charging techniques in a constrained charger infrastructure, according to [27], can lengthen the avg recharging times, resulting in higher peak load. EVs are powered by electric machines and are supplied directly from a source of energy rather than indirectly through an internal combustion engine., according to [28] (ICEs).Controlling a grids-attached converter in a bi-directional batteries chargers for use in plug-in hybrid EV was given by [29]. This is it. Electric vehicles are more pollution-free than traditional fossils fueled-powered cars, emitting less carbon dioxide, consuming less fuel, and polluting the air. Another benefit of EVs, according to [30], is that they may be utilized as power devices in both G to V and V to G applications when attached to their charger connectors. The core notion of the V to G technique has been explained by [31]. It includes automobiles as power devices and supplying power to the grids to keep the grid running during voltages instability and frequency drops. The key problems of EV batteries, according to [32], are safety, energy density cost, dependability, and life span. First and foremost, the EV prioritizes safety. The batteries' life durations can be assessed in two parts, according to [33]: the min calendars life and the charger-discharger cycles life. According to [34], trade-offs are taken into account on a priority basis, and an Electric Vehicles battery must fulfill all characteristics at reasonable expense Since the excessive cost of batteries has been a key barrier to Electric vehicles technology in the past.

2.4 Batteries of Electric Vehicles

According to [35], the high-density feature means that an EV with NiMH batteries has two operating ranges as one with lead-acid batteries. A Ni-MH battery has a longer life cycle since it can withstand mild overcharges and severe discharges. Because the Ni-MH battery has a low internal resistor, the charger efficiency is high. It also has higher costs and lowers charging acceptances capabilities in higher-temperature environments, lowering charger efficiency. "Taking account for Li-ion Battery deteriorations in EV Charger minimization," by [36]. For newer generations

of Electric Vehicles, such as the Nissan Leaf, lithium-ion batteries have become one of the preferred energy storage units. According to [37], Lithium-ion batteries are significantly less weight than other types of batteries and can deliver the same amount of capacity. For example, the AC Delco lead-acid battery pack in the Chevrolet Volt weighs 590 kg to supply the same amount of energy (16kWh), but the new Li-ion battery pack weighs just 170 kg, or 28.81 percent less than the original option. According to [38], the Li-ion battery pack has a significant number of cells. [39] introduced 48 modules with four cells each, totaling 196 cells in the Nissan Leaf battery pack.

2.5 Battery Charging of Electric Vehicles

[40] explain that not the battery design, but also the charger and discharger control impact battery performance. Batteries charging and discharging operations and controlling are typical techniques in the entire Electric vehicles devices. The constant voltage charger was proposed by [41]. To protect the battery, it requires an extra circuit.

Multiple constant current charging for the Constant current charger technique in solar battery charger was presented by [42]. Constant currents charge the battery with a set of currents, and the battery's voltage increases gradually with time. CC-CV charging technique was presented by M. Chen and G. A. Rincon-Mora[43]. Lithium-ion batteries have a max chargings voltage of 3.6V or 4.2V, according to [44].The CV stage begins when the V_{bat} hits 90% SOC, and the current begins to drop.

2.5.1 Onboard and off-board charger

[45] proposed bi-directional non-isolated DC-DC converters for quick EV chargers. Off-board charging stations may preferably extend the ranges of batteries in Electric Vehicles. EV With Traction-to-Auxiliary Mode Onboard Reconfigurable Batteries Charging was given by [46]. [47] used photovoltaic PCS systems to create both directional batteries charging for EVs. Minimal Charger Approaches for one direction V2G [48] by E. When an electric car is parked, its battery may be used as a source of energy, implying that significant numbers of EVs connected to the grid have a strong chance of operating as distributed power devices and feeding energy back to grids. A review on the Electricity generation of Transport in Smart Grids Environments was given by [49].

2.5.2 Onboard Bidirectional Charger

Plug-in Hybrid EV Charger techniques for max power Savings were provided by [50]. Electric Vehicles with both directions of battery chargings may be linked to the smart grids in this way, which will have a significant impact on the energy market. 3-phase bi-directionals batteries chargers for smart electric cars was developed by [51]. The Isolations Controlling ports of Three-Ports Bi-directional Converters for Electric Vehicles was provided by [52]. To guarantee galvanic isolation and safe operation, isolate transformers are frequently used between the grid sides and the battery packs. Designing, modeling, and implementation of a both-directional step-down and step-up converter were given by [53].

2.6 Soft Switching

Soft-switching approaches in PWM converters were presented by [54]. The output voltages or currents of traditional pwm DC-DC converters is typically controlled by producing gate pulses for the switching system, that is,by turn on diagonals pair of switch during the On stage and shutting off all the switch at the time of OFF stage. Three-level LLC series resonance DC-DC converter was given by [55]. High switching losses of power equipment and EMI emissions would occur from a high switched frequency. which would therefore decrease the conversion efficiency. Soft-switching technology, such as ZVS and ZCS, is commonly used to address this problem. ZCS operation was carried out by [56]. To reduce the substantial energy loss produced by the current during the turning-off time IGBT devices are preferred.

2.7 LLC Resonant Converter

LLC resonance converter for front-end DC-DC converter was given by [57]. The resonance tank of an LLC resonance architecture is made up of a series inductance, a series capacitance, and a magnetizing inductance. This converter with load short circuit protections have been developed by [58]. There are two resonant frequencies in the resonant tank because of the three components: one is tied to series inductance and capacitance, and the other is dictated by all elements. This converter utilized in the solar array simulator was provided by [59]. The resonant converter may accomplish soft switched characteristics while operating in the period above the resonance frequency, considerably decreasing switching and conduction losses. A bi-

directional LLC resonance converter for vehicle applications has been reported by [60]. ZVS in main side switch and ZCS in the rectifier, diode may be obtained with the LCL resonance tank in the DC-DC converters under all load situations, including no load. As a result of these benefits, it is obvious that the LLC resonance converters are a suitable technique that will be selected as the primary design choice in this study.

CHAPTER 3

Modelling and Analysis of High Gain Luo Converter for EV Battery Charging

3.1 Introduction

As explained in Chapter 1, full-bridge DC-DC converter with high-frequency isolated transformers and switches are commonly employed in the DC-DC stage of a common onboard Electric Vehicles battery charging circuit, as shown in Fig. 3-1 [9].to provide isolation between the supply-end converter and the EVs batteries [10] isolations and installation flexibility on electric vehicles. A Luo converter is a common choice of dc-dc converters because it has such an excellent voltage regulating feature within immediate changes in input voltage and better low loads efficiency. standard non-isolated inverted output Luo converters [5-7] give adequate results in terms of power quality, with higher Voltage level gain, improved currents, and voltage ripples characteristics.

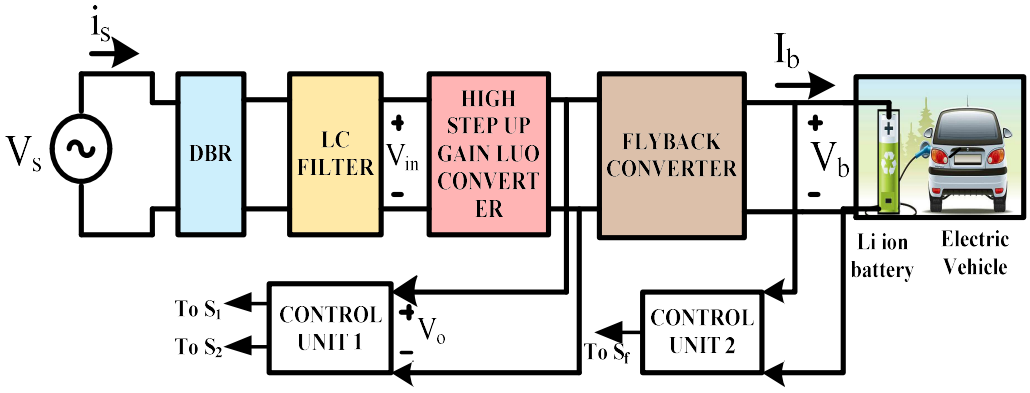

Fig. 3-1 Schematic Diagram of System

3.2 Objective

This chapter describes the basic operation of the High gain LUO converter. The main objective of this chapter is:

a) Power factor correction of circuit
b) High voltage gain
c) Reduction in THD%

3.3. Architecture of Luo Converter

The frameworks of the Electric Vehicle chargers have high stepping-up gain Luo converters and standard Luo converters shown in figures 3-2 (a) and 3-2 (b). This converter is made by dividing the input side inductance i.e. L_i into two halves and accruing one extra switch S_2 to a standard Luo converter. As a result, the switched inductor structure consists of two inductors $L_{1,2}$ with switches $S_{1,2}$ at the supply side. With diode D_o, the capacitors C_1 and an output inductance L_o, operate in a standard way. It has four-stage as follows:

- DBR
- Filter
- PFC converter stage
- Flyback converter

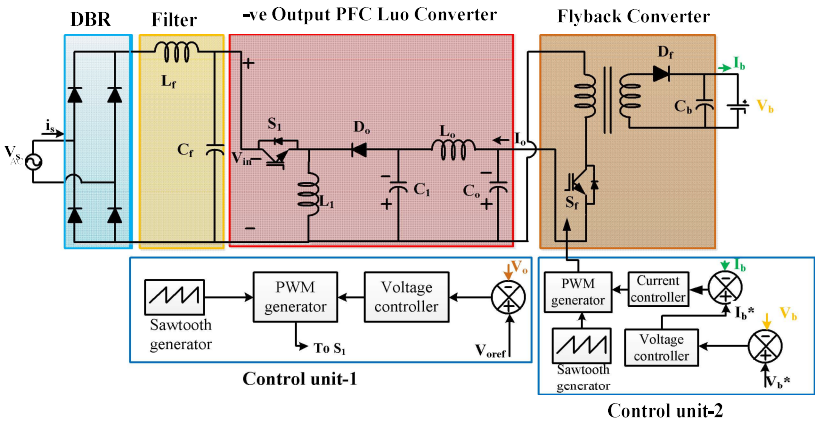

(a)

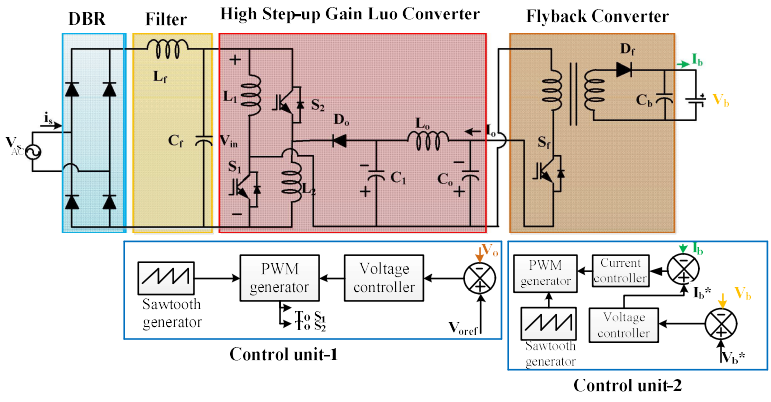

(b)

Fig. 3-2 Charger architecture based on (a) conventional Luo PFC converter (b) High gain Luo converter

DBR: A diode bridge rectifier is a special type of rectifier that converts alternating

current (AC) into direct current (DC). As alternating current can reverse direction periodically, as direct current consistently flows in a single direction, making it simple to control.

Filter: The filter is a device that is used to eliminate the ripple or fluctuation in DC voltages for achieving a complete smooth DC voltage at the output.

Flyback Converter: A flyback converter is employed to manage the battery current in constant voltage - constant current mode. The Flyback converters use very few components compared to the other types of SMPSs.

3.4 Design Specification of EV charger

Designing parameters of EV chargers are given below:

- Input Voltage: 360V DC
- Output Voltage: 52V

Table 3.1 SPECIFICATIONS OF HIGH GAIN LUO CONVERTER

S.NO.	Specification	High gain Luo converter
1.	Input voltage	220V single-phase AC
2.	Filter inductance	0.6mH
3.	Filter capacitance	0.9µF
4.	Input inductance	0.16mH
5.	Series capacitor	5µF
6.	DC link capacitor	250µF
7	Battery rating	48V/100Ah
8.	Output capacitor	1300µF
9.	Output inductance	3.57mH
10.	Switching frequency	20kHz
11.	Output power	700W
12.	Output voltage/current	360V/2.5A
13.	Current ripples in the output inductance	20%
14.	Voltage Ripples in series capacitance	10%
15.	Voltage Ripples in DC-link capacitance	3%
16.	Voltage Ripples in Output capacitance	0.1%

3.4.1. Modes of Operation

- Mode1: When both switches S_1 and S_2 are switched off at an identical time, this mode is activated. As demonstrated in Figs. 3-3(a) and 3-3(b), the inductances L_1, and L_2 begin to store energy from the source. The capacitor C_1 begins to discharge, transferring energy to the output through the inductance L_o. At this instant, the output diode D_o is in reverse bias.
- Mode2: Both switches S_1 and S_2 are switched off at the identical time. The output diode D_o enters the conducting conditions, as shown in Figs. 3-3(a) and 3-3(c). The stored energy is released via the inductors L_1, and L_2 and the transfer capacitance C_1 starts charging in the reverse direction. During this period, the load current is energized by the diode D_o, via inductors L_o and L_1, L_2.
- Mode3: Because none of the switches are conducting, this is termed DCM or freewheeling time. The stored energy in the inductances L1 and L2 is entirely drained, as seen in Figs. 3-3(a) and 3-3(c). Via the inductance Lo, and DC-link Capacitor Co give sufficient energy to the load via the transfer capacitor C1.

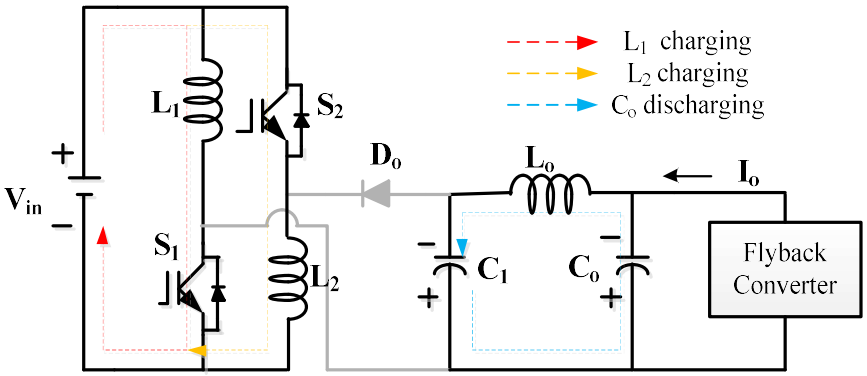

(a)

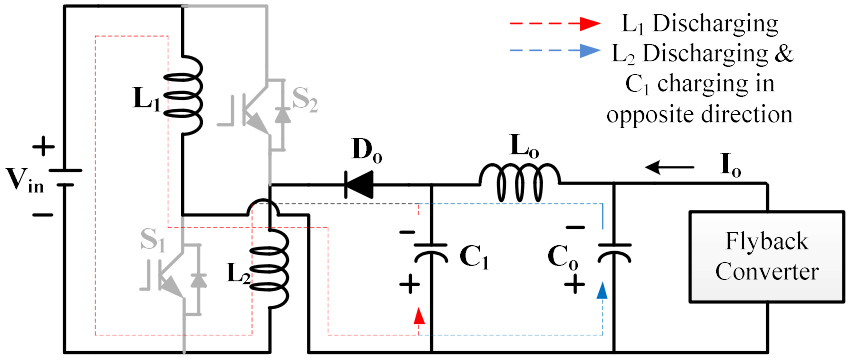

(b)

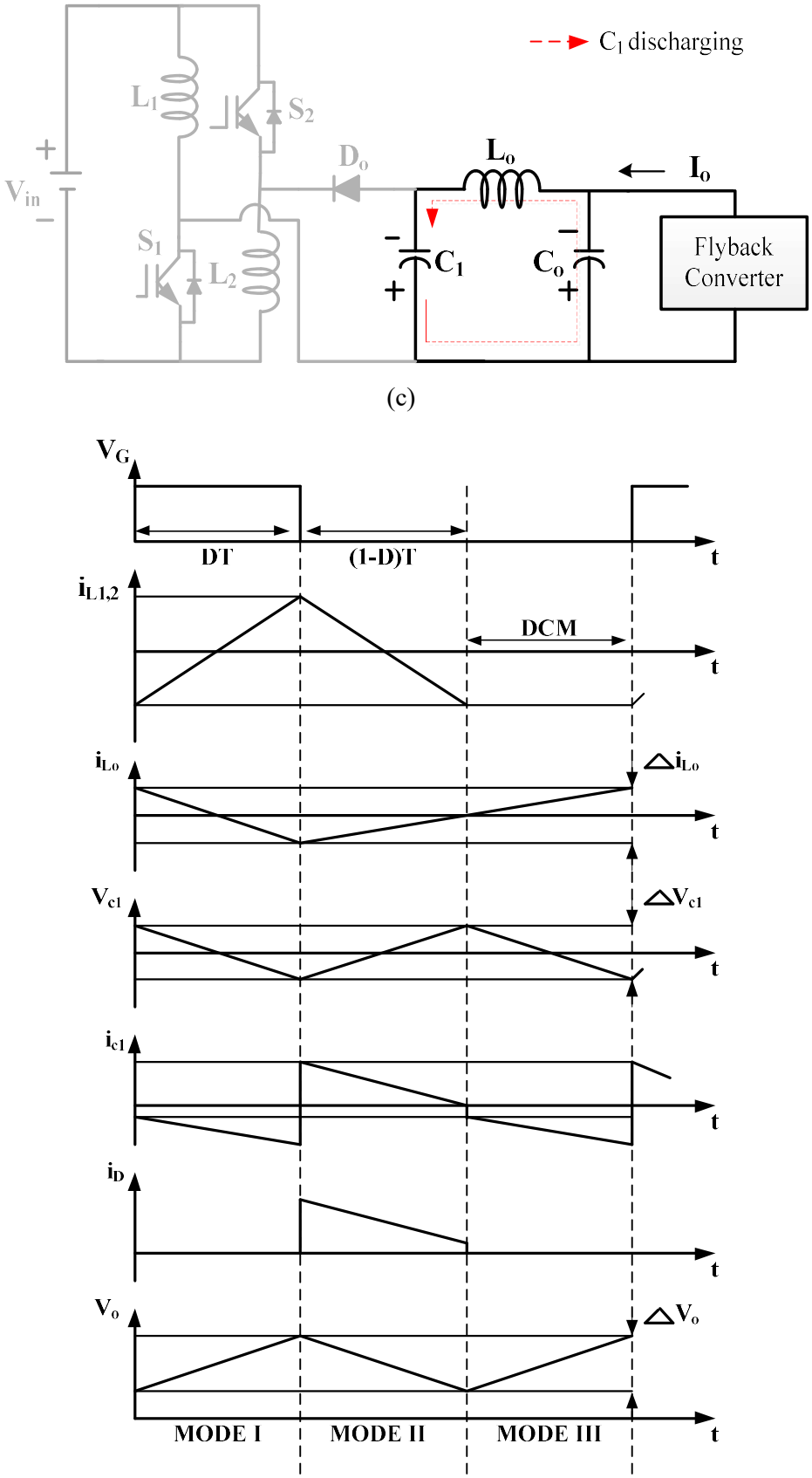

Fig. 3-3 (a)-(d) Operating Principle of high gain Luo converter over one cycle

During mode1 and mode2,

$V_{L1} = V_{L2} = V_{in}$ (1)

$V_{L1} = V_{L2} = \frac{Vo}{2}$ (2)

The transfer voltage is given as:

$\frac{Vo}{Vin} = \frac{2D}{(1-D)}$ (3)

The maximum voltage stress between switches and diodes can be calculated using the formula:

$V_{S1} = V_{S2} = V_{in}$ (4)

By applying KVL in loop, D_o-L_2-L_1-C_1, voltage stress across the diode is given as,

$V_{Do} = V_{in} + V_o$ (5)

The peak values of the switches and diode voltage stresses are relatively smaller than that of a traditional Luo converter ($V_{S1}=V_o$, $V_{Do}=V_{in}+V_o$) because achieving necessitated duty ratio is lesser than in a standard DCM converter, due to the smaller supply voltage put in for the same output voltage.

3.4.2. Computation of Design Parameters

To achieve PFC at the supply end of the EV chargers, a high gained Luo converter coupled with a flyback converter is developed in DCM. In DCM, the flyback converter is designed traditionally using the techniques described in [7]. Using expression (3) to consider the instantaneous supply voltage V_{in}, the equation of duty ratio D(t) is as follows:

$D(t) = \frac{Vo}{2V_{in}(t)+V_o}$ (6)

According to equation (6), these converters should perform with reduced AC input voltage to give stepping-up operations for specific DC-link voltage and power rating, equivalent to the standard Luo converter. As a result, the Luo converter is built for voltage conversion from 220V AC to 360V DC, with a range of 200V (V_{smin}) to 250V (V_{smax}).

3.4.2.1. Design of High Gain Luo Converter

It is supplied by DC voltage generated at the output of DBR and EMI filter i.e. average output is indicated as V_{in} and is given as follows:

$V_{in} = \frac{2\sqrt{2}V_s}{\pi} = \frac{2\sqrt{2}*220}{\pi} = 198V$ (7)

V_s is the input voltage. At the input, the converter has two inductors L_1 and L_2 which are designed to work in Discontinuous Conduction mode. As a result, the critical value of $L_{1,2}$ is determined as follows:

$$L_{1,2} = \left(\frac{V_{s\,min}{}^{\circ}}{Pi}\right)\frac{T_s}{2}\frac{V_o}{2V_{s\,max}\sqrt{2}+V_o} = 0.16mH \quad (8)$$

The critical value of a series capacitor is given by:

$$C_1 = \frac{Pi}{\xi f_s(2\sqrt{2}V_{s\,max}+Vo)^{\circ}} = 5\mu F \quad (9)$$

The critical value of the output inductor of the converter is given as:

$$L_O = \left(\frac{V_{s\,min}{}^{\circ}}{Pi}\right)\frac{T_S}{\delta}\frac{V_O}{2V_{s\,max}\sqrt{2}+V_o} = 3.57mH \quad (10)$$

The value of filter inductance and filter capacitance is given by:

$$L_f = \left[\frac{1}{(4\pi^{\circ}f_c{}^{\circ}C_f)}\right] - \left[\frac{(0.04V_s{}^{\circ})}{(2\pi f.P_i)}\right] = 0.6mH \quad (11)$$

$$C_{f\,max} = \frac{(P_i.\mathrm{Tan}\theta)}{(2\pi\ .V_s{}^{\circ})} = 0.9\mu F \quad (12)$$

DC link capacitor i.e. output capacitor of high gain Luo converter is given as:

$$C_O = \frac{P_i}{(4\pi f V_o \Delta V_o)} = 250\mu F \quad (13)$$

3.4.2.2. Design of Flyback Converter

It is designed by a transformer that provides isolation, a diode D_f and a capacitor at the output. Selecting the correct magnetizing inductance L_m in the operation of high-frequency transformers and flyback converters L_m is very significant. It is assigned a value that is significantly lower than the calculated critical value. L_m is given by:

$$L_{mf} = \frac{(V_o D_f)^{\circ}}{(2V_b I_b f_{sw})} = 240\mu H \quad (14)$$

An output capacitor of flyback converter C_b is used to keep the output current ripple to a minimum value. It can be calculated as follows:

$$C_b = \frac{D_f V_b}{f_{sw}(\frac{V_b{}^{\circ}}{P})\lambda V_b} = 1300\mu F \quad (15)$$

Duty cycle of flyback converter operation is:

$$D_f = \frac{V_o}{\frac{n_s}{n_p}V_b + V_O} \quad (16)$$

3.5 Fractional-order PI controller for High gain Luo converter

A FOPI controller has been designed to control and maintain the voltage across the DC-link. The invention of the FOPI controller is primarily due to advances in

fractional calculus [9]. A FOPI controller differs from a PI controller in that it uses a changeable non-integer order of integral components while a PI controller only uses one. The FOPI controller's structure is as follows:

$$F(s)=K_p + K_i/(s^{\wedge}\lambda) \quad (17)$$

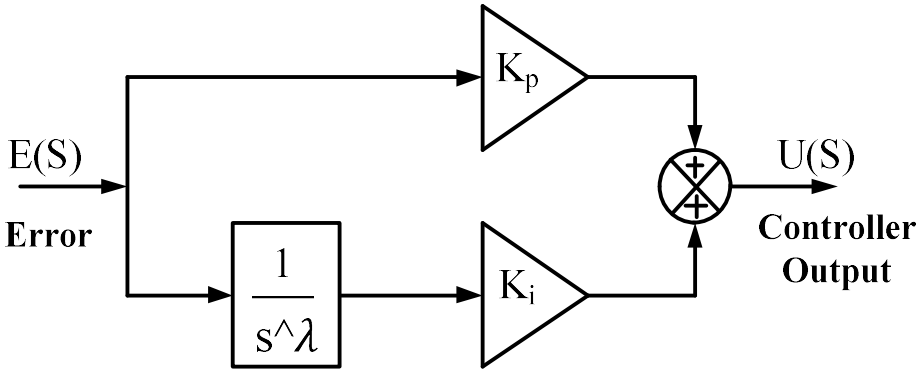

Fig. 3-4 Block diagram of fractional-order PI

In CC and CV modes, the Luo converter requires a potential regulator technique for DC-link potential regulation, and a flyback converter is regulated for small ripples-based charging batteries. The following are the controls for two converters:

3.5.1. High Gain Luo Converter Control

In Fig. 3-5, the DC link voltage V_o developed at the output end of the High gain Luo converter which is compared to the reference DC voltage i.e.V_{oref} regulating, and given to the voltage FOPI controller.

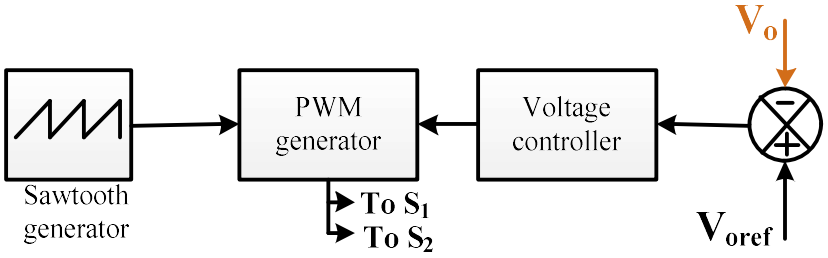

Fig. 3-5 Control unit of High gain Luo converter

3.5.2. Flyback Converter Control

In Fig. 3-6, the controlling of a flyback converter requires a dual loop control of fractional order proportional integral in which the battery voltage V_b is measured and compared to a constant voltage taken as reference i.e.V_b*, and the resulted value is given to a voltage FOPI controller and connected in series with a current fractional-order proportional-integral controller which helps to generate controlled pulses for

the flyback converters switch.

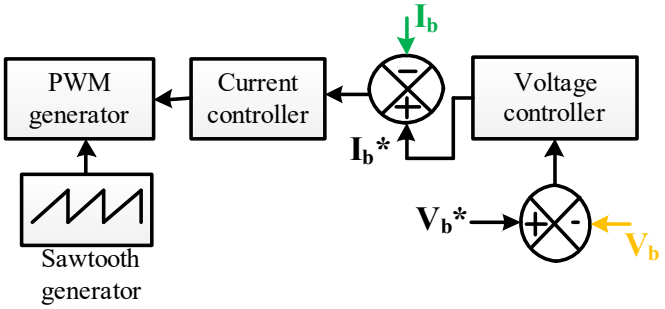

Fig. 3-6 Control unit of Flyback converter

Various ways can be employed for perfect fractional order proportional integral tuning. For the very same, the Ziegler Nicholas approach is employed. First, the transfer function is derived using steady-state analysis and state-space modeling, and then the value of the critical constant K_{cr} is calculated using the Routh Hurwitz criteria, which aids in the computation of the auxiliary equation and the determination of T_{cr}. The values of K_p and K_i can be found by using the following formula:

$$K_p = 0.45K_{cr} \tag{18}$$

$$Ki = (1.2*K_p)/T_{cr} \tag{19}$$

Selected values of Kp and ki are 0.232 and 20 respectively and the order of integration λ=0.455.

3.6 SIMULATION RESULTS

Fig. 3-7 depicts the Simulink model of the High gain Luo Converter circuit. The output voltage is controlled by the fractional PI controller.

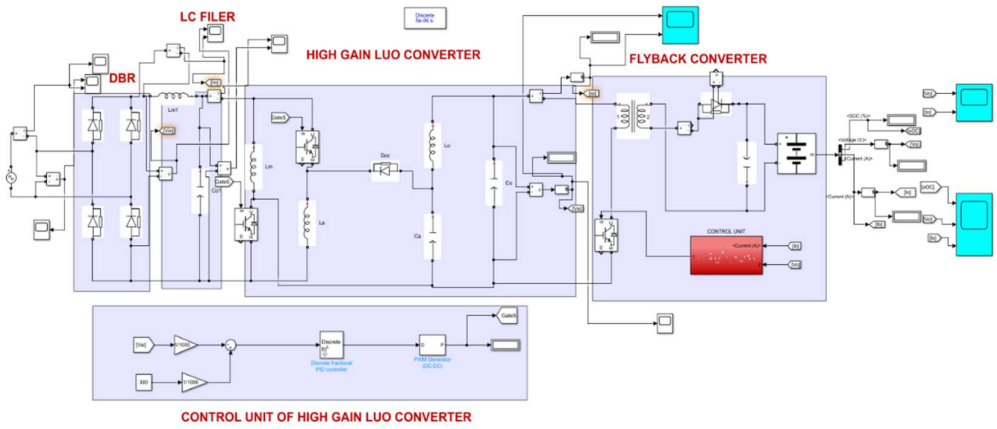

Fig. 3-7 simulation of high gain Luo converter

The device shows the values of different variables of a 48V, 100Ah Li-ion battery that is being charged by the developed framework. supply voltage, supply current, Battery voltage, SOC%, and battery current are represented in Fig. 3-8. (a)-(c). Supply voltage and current both are in phase in Fig. 3-8. (a),indicating that the circuit has power factor correction. In Fig. 3-8.(b) output of Luo converter i.e. voltage and current across the DC link capacitor. The battery charges gradually as the SOC% increases in Fig. 3-8. (c). Figure 3-9 depicts the fluctuation in THD in the system, which is lower than 5%. With a steady current of 12A, the battery is charged to a constant voltage of 52V. A negative current value indicates that the battery is being charged. The performance of the system is given below:

3.6.1. Supply Performance

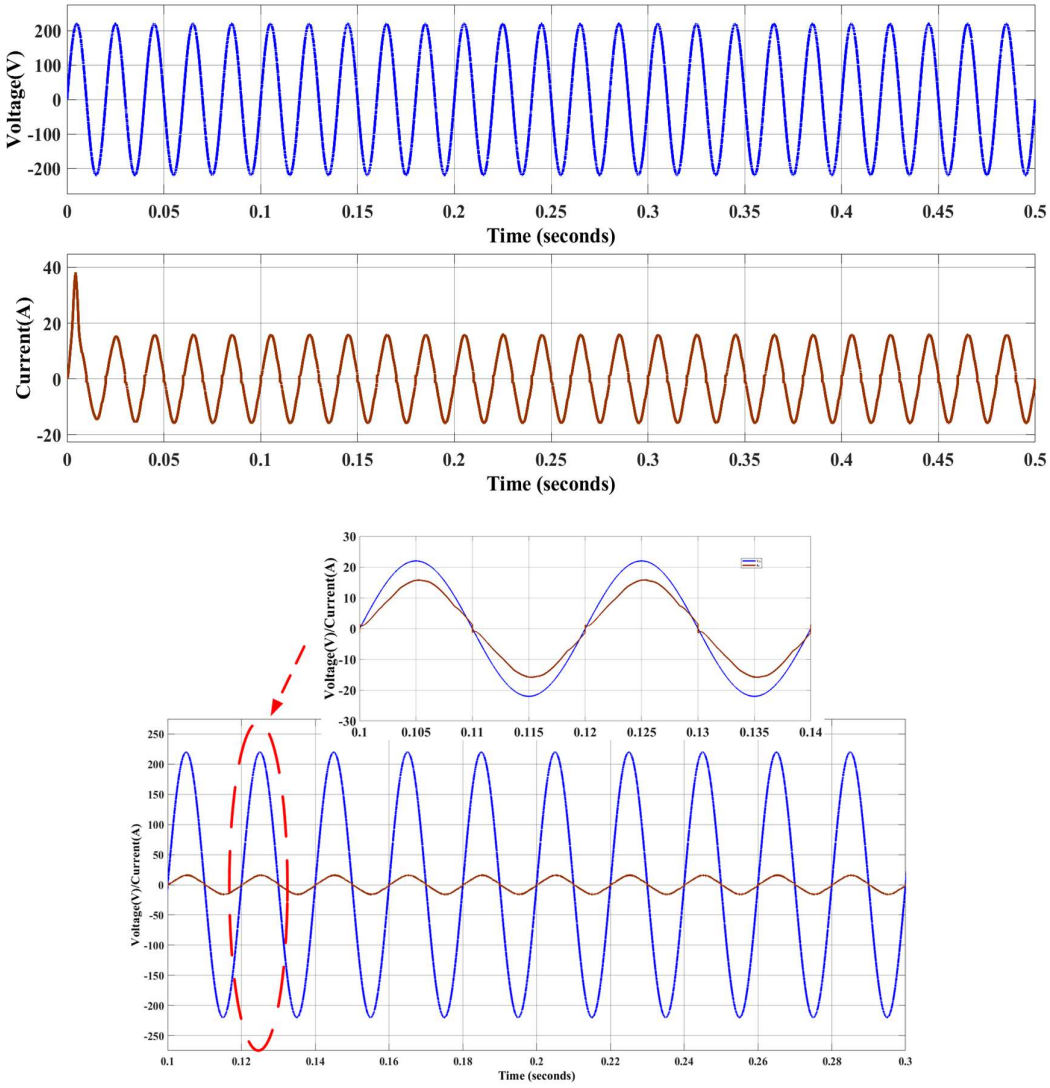

Fig. 3-8(a) Input Current(A), Input Voltage(V)

3.6.2. Luo Converter Performance

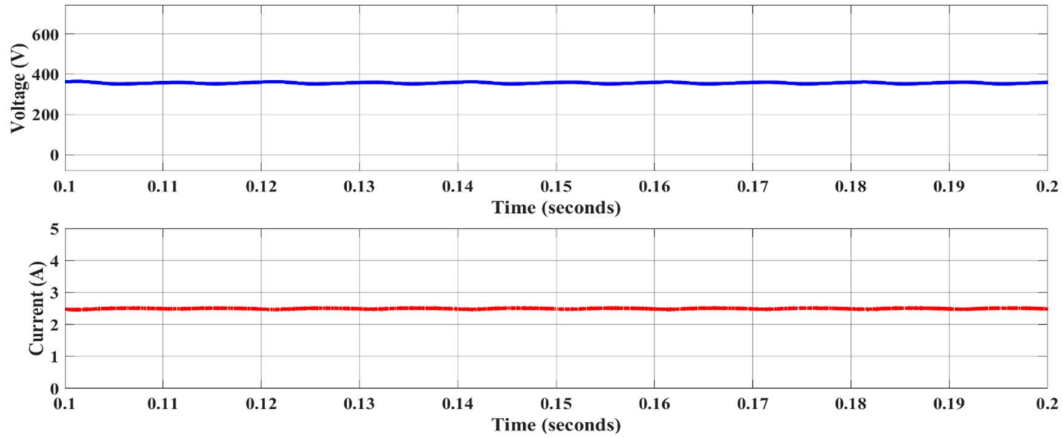

Fig. 3-8(b) Output Voltage(V), Output Current(A) of High gain Luo converter

Voltage and current across each parameter of the high gain Luo converter are shown below:

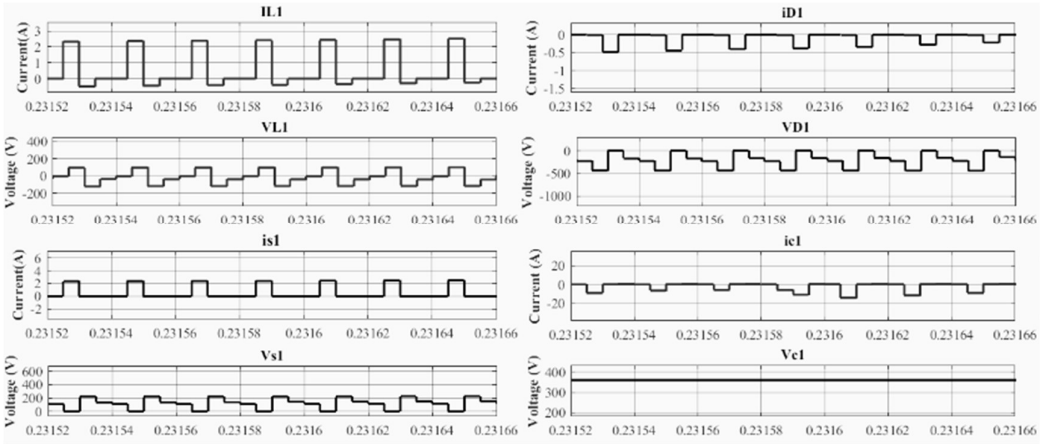

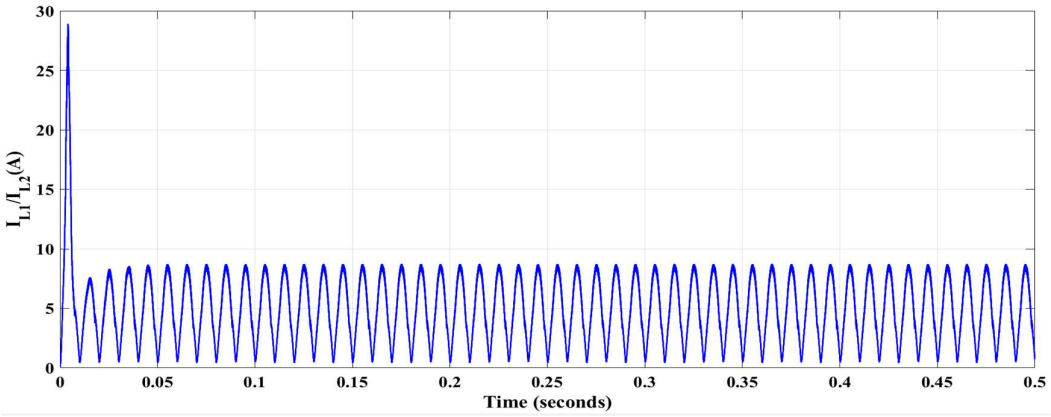

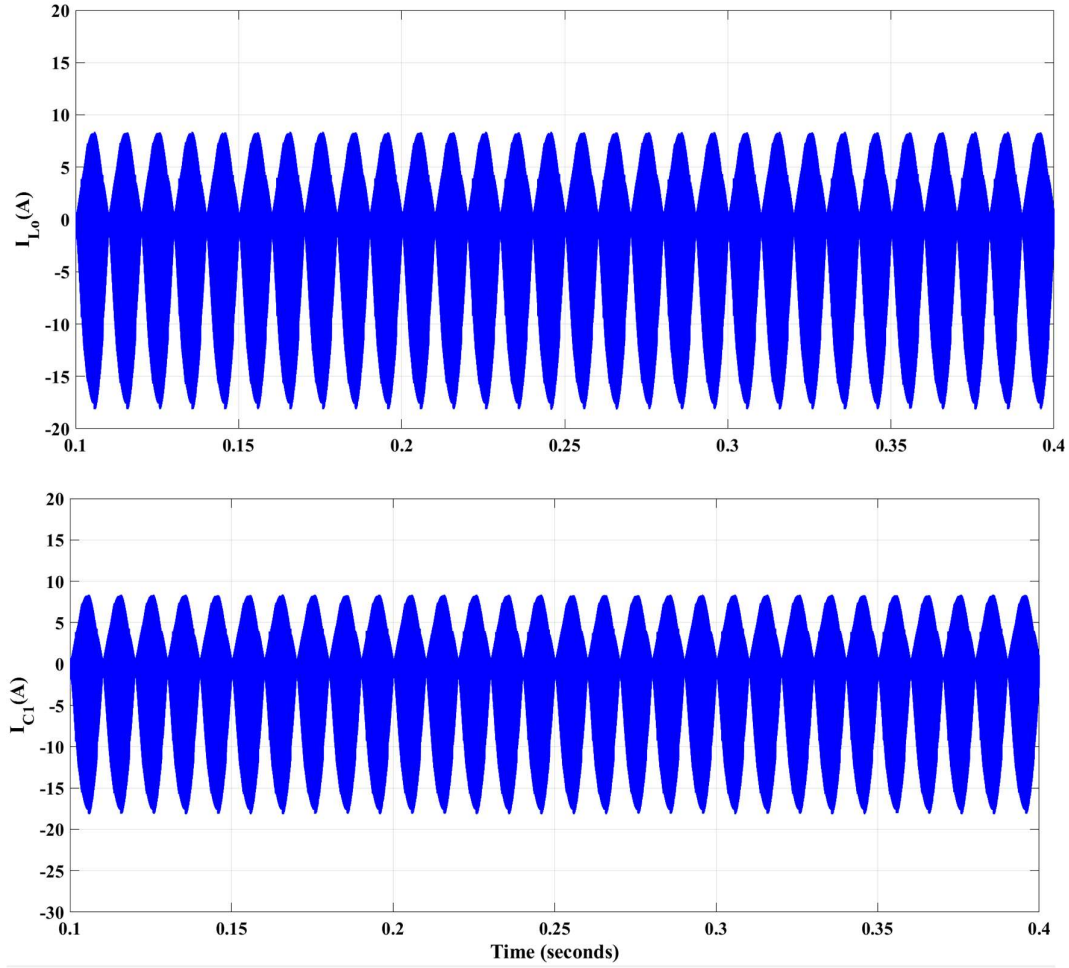

3.6.3. Battery Performance

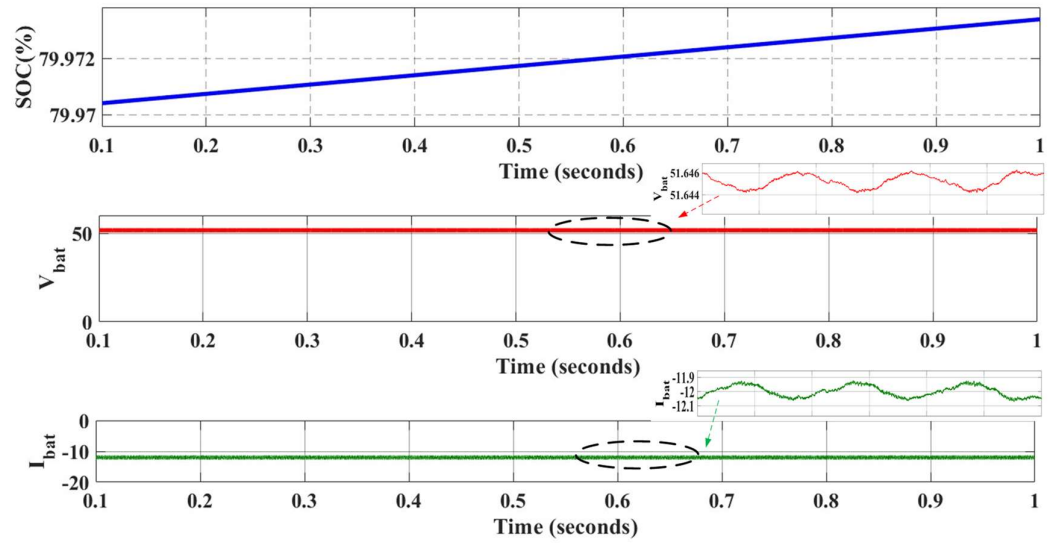

Fig. 3-8(c) SOC%, Battery Voltage(V) and Battery Current(A)

THD fluctuation among different topologies connected to Luo can be noticed in Fig. 3-10. It shows how a high gain Luo converter reduces the Total harmonic distortion of supply current, making the device more fuel-efficient. The power factor varies with load change and various converter topologies, as shown in Fig. 3-11. It can be observed that with a high gain Luo converter, approximately unity power factor is obtained, and the significance of the power factor correction unit is also clearly obtained.

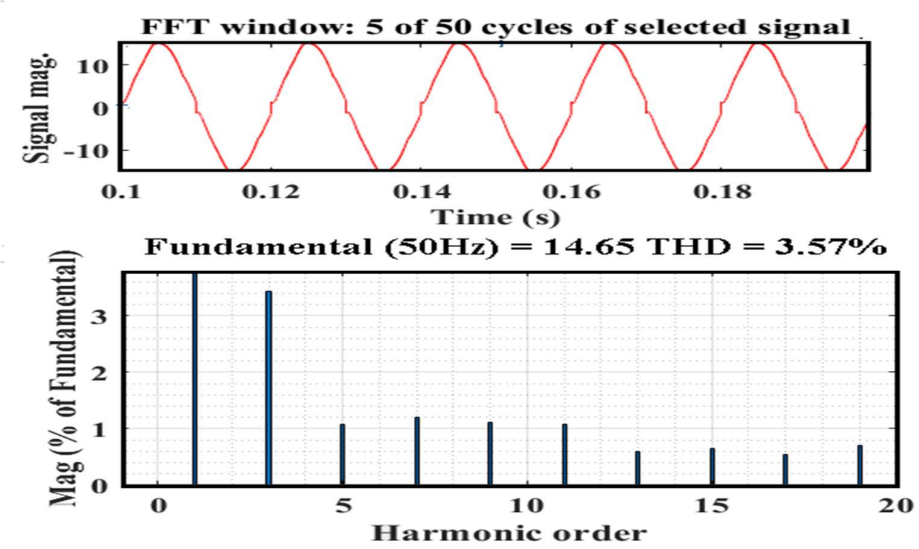

Fig. 3-9 Input Current THD

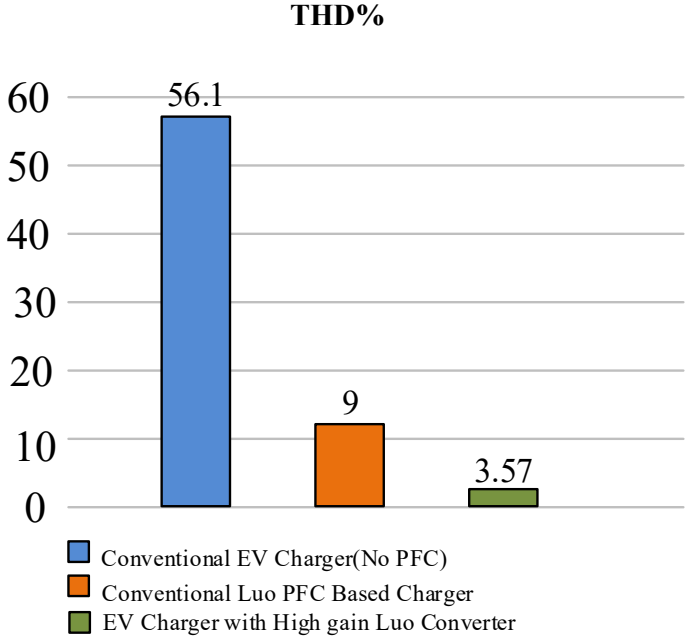

Fig. 3-10 THD Comparison

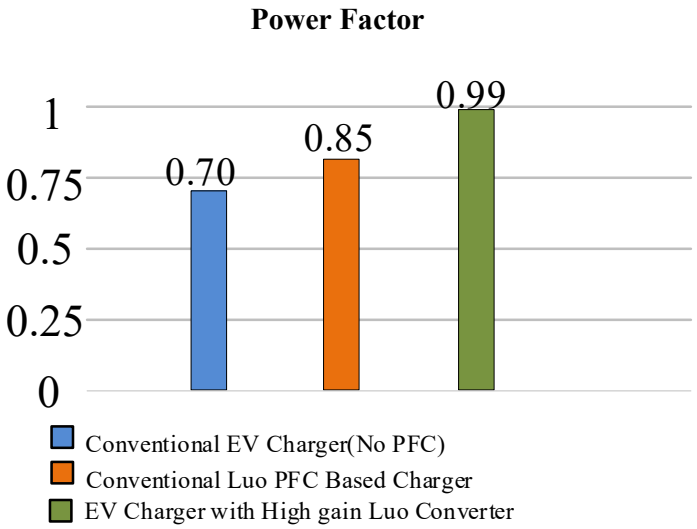

Fig. 3-11 Power Factor Comparison

3.7 CONCLUSION: This chapter presents a high stepping-up gain Luo converter with decreased system stress for PFC at the front-end of an EVs batteries charger. This reduction in switch voltage is produced in the conventional Luo converter by installing one switch and splitting the input inductor. The advantage of this converter over standard boost and Luo PFC converters in producing the same DC-link voltage is achieved in terms of fewer system stresses, as this Luo converter operated at a low duty ratio due to the input switching inductors design. This high gain Luo converter is suitable for high-power EV chargers since the switching voltage and current stresses are massively decreased.

CHAPTER 4

Modelling and Analysis of Half Bridge LLC Resonant Converter for EV battery charging

4.1 Introduction

This work presents the topology for battery charging. The Half-Bridge LLC resonance DC-DC converter is the second step, which allows battery charging. the batteries output voltage is regulated using a Proportional-Integral (PI) controller and Pulse Frequency Modulation (PFM) algorithms.

4.2 Objective

This chapter describes the basic operation of the half-bridge LLC resonance converter for all the three modes of operations:

1. Below resonance mode
2. Resonance mode
3. Above resonance mode

4.3 Architecture of LLC

A Half-Bridge LLC Resonance converter is depicted in Fig.4-2. The components of this converter are as follows:

- Square wave generator
- Resonant circuit
- Rectifier circuit

A battery charger for an electric vehicle that uses Half-Bridge LLC resonance converter in the second stage is shown in fig.5-1.

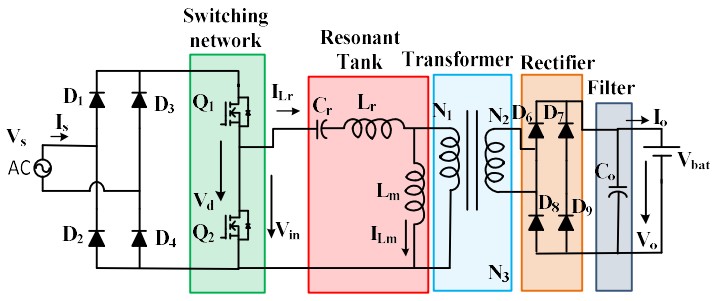

Fig. 4-1 Presented Half-Bridge LLC Resonant Converter

The half-bridge generates square wave voltage, Vd, by operating the MOSFET switches Q_1 and Q_2 alternately with a duty ratio of 50% for Q_1 and Q_2. A tiny amount of dead time is usually provided between each transition.The resonant network circulates and passes energy to the output via the transformer. A bipolar square wave is obtained at the transformer's primary coil, and this voltage is transmitted to the secondary coil with the turn ratio for the required output voltage.

4.3.1 Transfer Function of LLC Resonant Converter

Transfer gain = switching bridge gain* gain of the resonant tank* turn ratio (N_1/N_2). The switching bridge gain for a full bridge is 1 and for a half-bridge is 0.5. Analysing the equivalent resonant circuit depicted in Figures 4-3 yields the resonant tank gain.

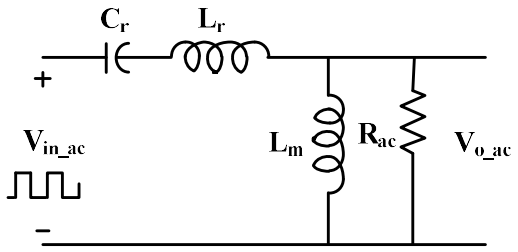

Fig. 4-2 Equivalent resonant circuit

The resonant tank gain is the magnitude of its transfer function as:

$$K(Q, m, F_x) = \left| \frac{V_{O_{ac}}(S)}{V_{in_{ac}}(S)} \right| = \frac{F_x^2 m}{\sqrt{(m+1).(F_x^2-1)+j.(F_x^2-1).F_x m.Q}} \quad (1)$$

Normalized switching frequency:

$$F_x = \frac{f_r}{f_s} \quad (2)$$

Series resonant frequency:

$$f_r = \frac{1}{2\pi\sqrt{L_r C_r}} \quad (3)$$

Parallel resonance frequency:

$$f_p = \frac{1}{2\pi\sqrt{(L_m + L_r)C_r}} \quad (4)$$

Quality factor:

$$Q = \frac{\sqrt{Lr/Cr}}{R_{ac}} \quad (5)$$

Reflected load resistance:

$$R_{ac} = \frac{8}{\pi^2} \cdot \frac{N_P^2}{N_S^2} \cdot R_0 \quad (6)$$

Inductance ratio:

$$m = \frac{L_m + L_r}{L_r} \quad (7)$$

Magnetizing Inductor:

$$L_m = \frac{2\pi f_r m Q N_s^2}{N_p^2 R_o} \quad (8)$$

Resonant Inductor:

$$L_r = \frac{1}{(2\pi f_r)^2 C_r} \quad (9)$$

Resonant Capacitor:

$$C_r = \frac{1}{2\pi Q f_r R_{ac}} \quad (10)$$

Load Resistance:

$$R_o = \frac{V_0^2}{P_0} \quad (12)$$

4.4 Mode of Operation

It is divided into three modes [9] on the basis of switching frequency as shown in fig.4-4:

- $f_s < f_r$: Boost mode
  - $f_s = f_r$: Resonant mode
  - $f_s > f_r$: Buck mode

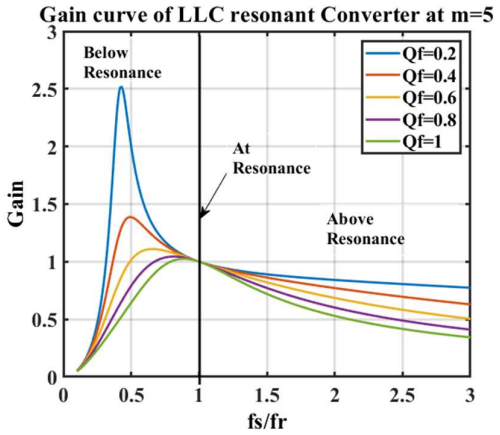

Fig.4-3 mode of operations

In the switching period, the converter can do two operations, as explained below.

1. The equivalent circuit of this model is shown in Figures 4-5. In a switching period, the power delivery operation happens in two ways: firstly, when the resonance tank is energized by positive voltage, causing the current to resonate in the positive direction during the first half of the switching period.

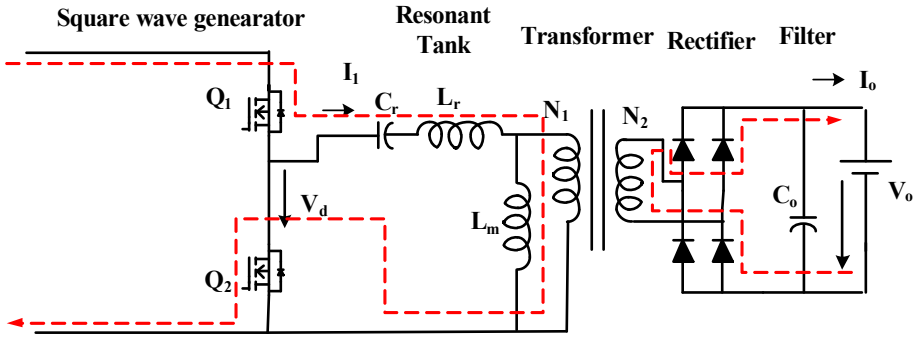

Fig. 4-4 Positive half of switching cycle

Second, when the resonance tank is activated by a negatively voltage, the current in the second half of the switching period, as shown in Fig. 4-6, resonance in the negative direction. At power supply processes, the magnetising inductance voltage is the positively/negatively reflected output voltage, and the magnetising current is charging/discharging.

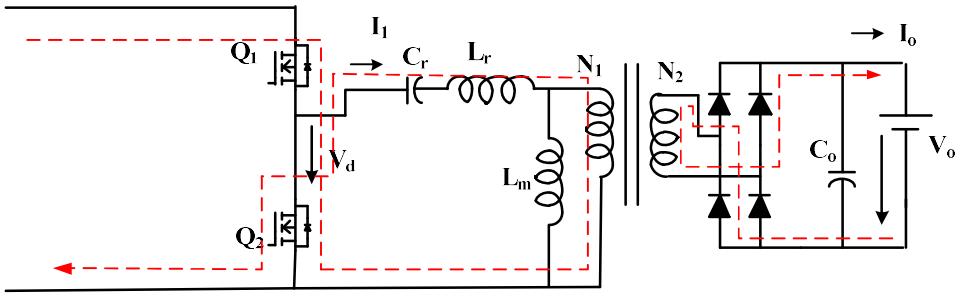

Fig. 4-5 Negative half of the switching cycle

2) Only when the resonance current is equal to the transformer magnetization current, which only occurs when fs<fr, causing the transformer secondary winding drop to zero and the secondary side rectifier to unplug, causing the transformer secondary current to The appropriate circuits for the freewheeling operation in both halves of the switching period are shown in Figures 4-7 and 4-8.

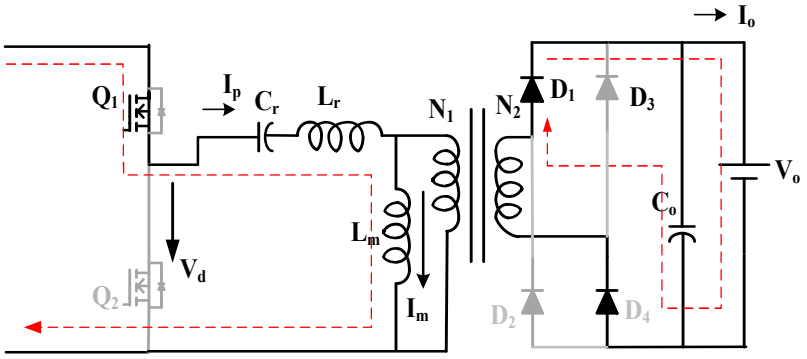

Fig.4-6 Positive half of freewheeling operations

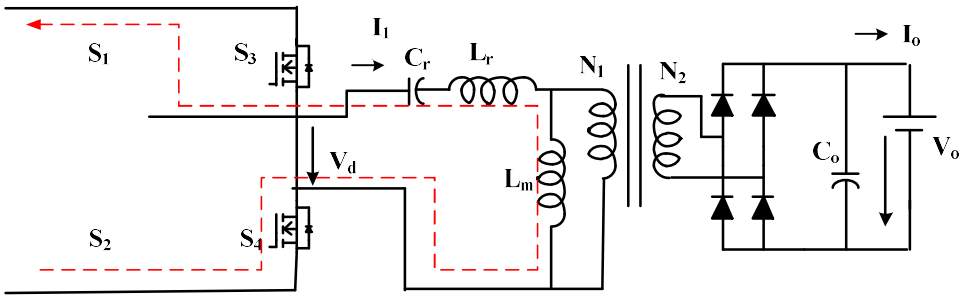

Fig.4-7 Negative half of freewheeling operations

4.4.1 At Resonant frequency operation fs=fr

The resonance half cycle is finished during the switching half cycle. At the end of the switching half period, the resonance inductance current I_{Lr} achieves the magnetization current I_{Lm}, while the rectifying current is zero. The turns ratio is selected so that the converter works at standard input and

output voltages at this point because the resonance tank has unity gain and gives the best operating and efficiency.

4.4.2 Above resonant frequency operation fs>fr

The slight power delivery procedure (described above) in each half of the switching period is similar to the resonance frequency procedure, but it is different in that the resonance half period is not completed and is affected by the start of the other half of the switching period, resulting in increased turn off losses in primary-side MOSFETs and hard commutation in secondary rectifier diodes. When a buck operation is necessary, the converter runs at greater supply voltage.

4.4.3 Below resonant frequency operation fs<fr

When the resonance half cycle is completed and the resonant inductance current I_{Lr} reaches the magnetization current, the freewheeling operation begins and continues to the end of the switching half period, in results conduction losses is increases on the primary side due to circulating energy. When a boosting procedure is necessary, the converter runs at a lower supply voltage.

4.5 Design of Half-Bridge LLC Resonant Converter

The design parameters are calculated in resonance mode:

Considering E_{ff} = 96%, input power (P_{in}) is computed as:

$$P_{in} = \frac{P_0}{E_{ff}} = \frac{700}{0.96} = 729W \quad (13)$$

The PFC output voltage is the max supply voltage (V_{OPFC}). PFC mainly employs a boost converter,

$V_{in}^{max} = V_{OPFC}$
(14)

$$V_{in}^{max} = V_{OPFC} = 420V$$

The lowest input voltage can be calculated using the Hold-up time (TH), which is the time needed to control PFC output regulated voltage.

$$V_{in}^{min} = \sqrt{420^2 - \frac{2 \times 729 \times 20 \times 10^{-3}}{470 \times 10^{-6}}} = 338.167\ V \quad (14)$$

For the optimum PFC output voltage, the LCL resonance converters are assumed to operate at the resonant frequency.

$$M^{min} = 1 \; at \; f_s = f_r \tag{15}$$

The maximum voltage can be computed as:

$$M^{max} = \frac{V_{in}^{max}}{V_{in}^{min}} M^{min} = \frac{420}{338} \times 1 = 1.24 \tag{16}$$

The turns ratio of the transformer is computed as:

The turn ratio can be calculated using the voltage drop V_X of 0.8V.

$$n = \frac{N_p}{N_s} = \frac{V_{in}^{max}}{2(V_0 + V_X)} . M^{min} = \frac{420 \times (1)}{2(58 + 0.8)} = 3.6 \tag{17}$$

Equivalent load resistance is calculated using the transformer turns ratio (n) as,

$$R_{ac} = \frac{8n^2}{\pi^2} \frac{V_0^2}{P_0} = \frac{8 \times 3.6^2}{\pi^2} \frac{58^2}{700} = 50.83\Omega \tag{19}$$

Resonant circuit parameters

The peak gain attributes described in [10] are utilized to establish the suitable Q and inductor ratio for determining resonant network parameters (m). It should be noticed that lowering the Q and m numbers results in a higher peak gain. The lower the m value, the lower the magnetizing inductance, resulting in poor transformer coupling, excessive circulating current, and decreased efficiency. To establish the optimum Q value, 10-20 % margins in max gain are taken into account when considering ZVS and load transient.

Mmax is 1.24 for the minimum input voltage (V_{inmin}). A max gain of 1.47 is needed with a 15% margin. Using the peak gain curve given in Fig. 4-9, Q is computed as 0.4 with inductor ratio(m) settle to 5. For the resonant frequency(fr) of 100kHz, the resonant components are.

The voltage controller utilized in APFC as an outer loop effectively controls the DC-link voltage (Vd). This $V_d$iswas applied to the Half-Bridge LLC resonant converter in the second stage. The design values of LLC resonant converter components are obtained using the specifications:

Supply voltage V_s: 220V

Supply frequency f_{supply} : 50Hz

DC-link Voltage V_d : 400V

Output voltage V_o : 48V

Output power P_o: 576W

Resonant frequency f_r : 70kHz

The turns ratio (T) is given as,

$$T = \frac{V_d}{2V_o} = \frac{400}{2 \times 48} = 4.16$$

The turns ratio is selected as 4.3 for operating LLC converter below resonance frequency. The peak current of the resonant tank is computed as:

$$I_{Lr} = \frac{2\pi P_o}{2V_d} = \frac{2\pi \times 576}{2 \times 400} = 4.52\ A$$

Resonance capacitor can be calculated as,

$$C_r = \frac{I_{Lr}}{2\pi f_r \, V_d/2} = \frac{4.52}{2\pi \times 70 \times 10^3 \times 400/2} = 51.4nF$$

For the suitable voltage gain of the LLC converter, the ratio of L_r and L_m is selected as 0.167. The resonant inductor and magnetizing inductance can be expressed as,

$$L_r = \frac{1}{(2\pi f_r)^2 C_r} = \frac{1}{(2\pi \times 70 \times 10^3)^2 \times 51.4n} = 100.6\mu H$$

$$L_m = \frac{L_r}{0.167} = \frac{100.6\mu H}{0.167} = 604\mu H$$

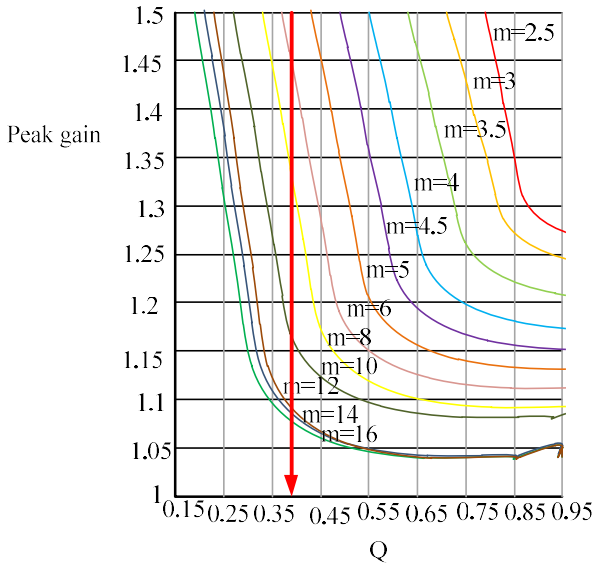

Fig.4-8 Peak gain characteristics w. r. t. Q for various m value

For the minimal nominal frequency, differentiate the gain M of equation (8) w. r. t. F_X and equated to zero, minimal frequency is described as,

$$\frac{dM}{dF_X} = 0 \Rightarrow F_X = 0.51$$
$$f_{min} = F_x \times f_r = 0.51 \times 100 \times 10^3 = 51kHz$$

4.6 Control Techniques of Charger

4.6.1 Pulse Frequency Modulation (PFM)

The PFM block architecture is in Figures 4-12, which is utilized to produce gate pulse for both Q1 and Q2. For a fixed duty ratio of 50%, the PFM varies the frequency.

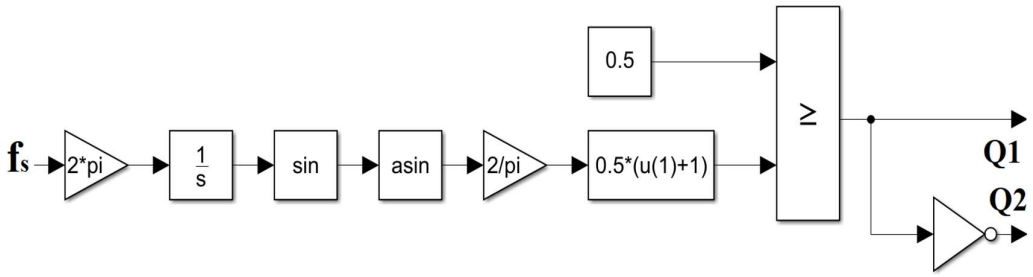

Fig.4-9 PFM Controller

4.6.2 LLC CONTROLLER

The LLC resonant converter receives the DC-link voltage, and the converter's output voltage is regulated by the PI-Controller. The output voltage (Vo) is compared to the reference output voltage (Vo*), and the resultant signal is processed by the PI-controller, which behaves as a voltage controller, and the Pulse Frequency Modulation (PFM) controller, which produces the switching pulse for the Half-Bridge LLC resonant converter.

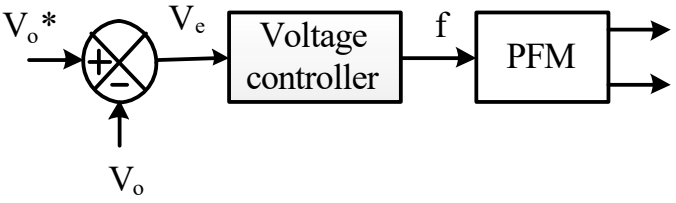

Fig. 4-10 LLC Controller

The proportional and integral gain for a various controllers is given below:

- Proportional-Gain of Voltage Controller (G_{pv}): 0.44
- Integral-Gain of Voltage Controller (G_{pi}) : 21.77
- Proportional-Gain of Current Controller (G_{pi}) : 7.00

- Integral-Gain of Current Controller (G_{ii}) : 1300
- Proportional-Gain of LLC Controller (G_{pllc}) : 500
- Integral-Gain of LLC Controller (G_{illc}) : 10,000

4.7 Simulation Result and Discussion

The evaluation of the proposed converter for electric vehicle battery chargers is discussed in this section. By adjusting the source input voltage and load changes, the proposed charger's steady-state performance is evaluated.

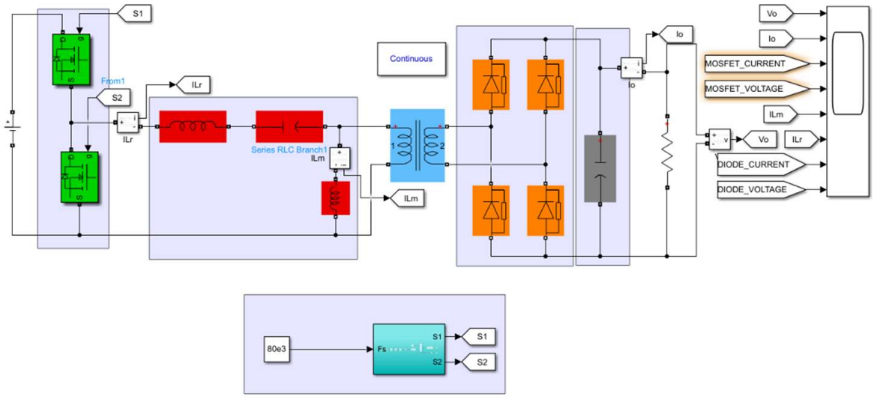

Fig. 4-11 Simulation block of PFC-boost fed Half-Bridge LLC resonant Converter

The transfer Gain curve for various values of Q at m=5 is presented in Fig.4-14w.r.t. standard frequency.

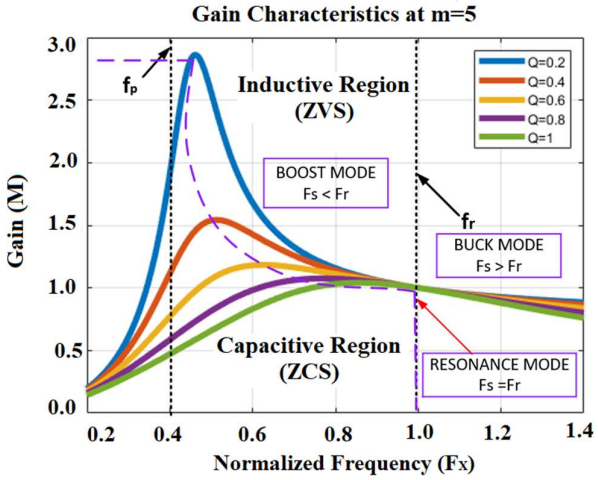

Fig.4-12 Gain M for different Q

As illustrated in Fig. 4-14, resonance frequency gain is unity, and running at this frequency is called a resonant mode of operations. The boost mode uses a converter with a switching frequency less than the resonance frequency and a gain larger than

one. In the buck mode, a converter's switching frequency is higher than its resonance frequency, and its gain is less than one.

4.7.1 Resonant Mode of Operation

This is depicted in Fig. 4-14 with the normalised frequency = 1 i.e. (fs=fr).

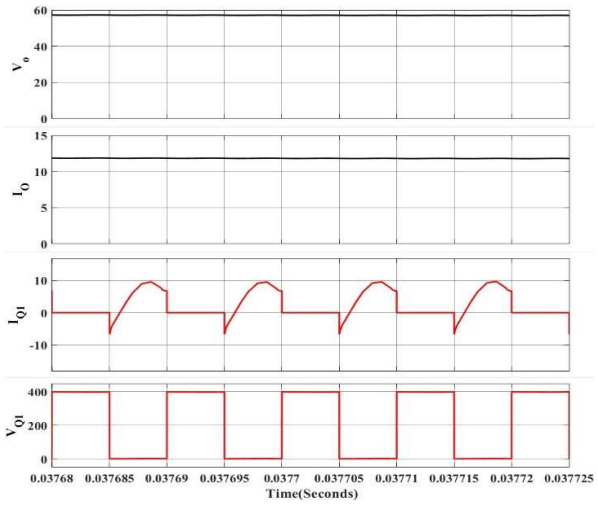

Fig.4-13 Output Voltage at resonance mode,Output Current at resonance mode, Mosfet current, and Voltage across MOSFET in resonance mode

The output voltage in Fig. 4-15 is 57.7 V, with a ripple of 120mV. The upper limit of 57.70V and the lower limit of 57.58V are calculated. the output current of 11.8 A with a ripple of 0.03 A. Simulation measured an upper limit of 11.8 A and a low value of 11.5 A. Mosfet current is also depicted in the Fig. 4-15.The peak voltage across Q_2 is 420 V.

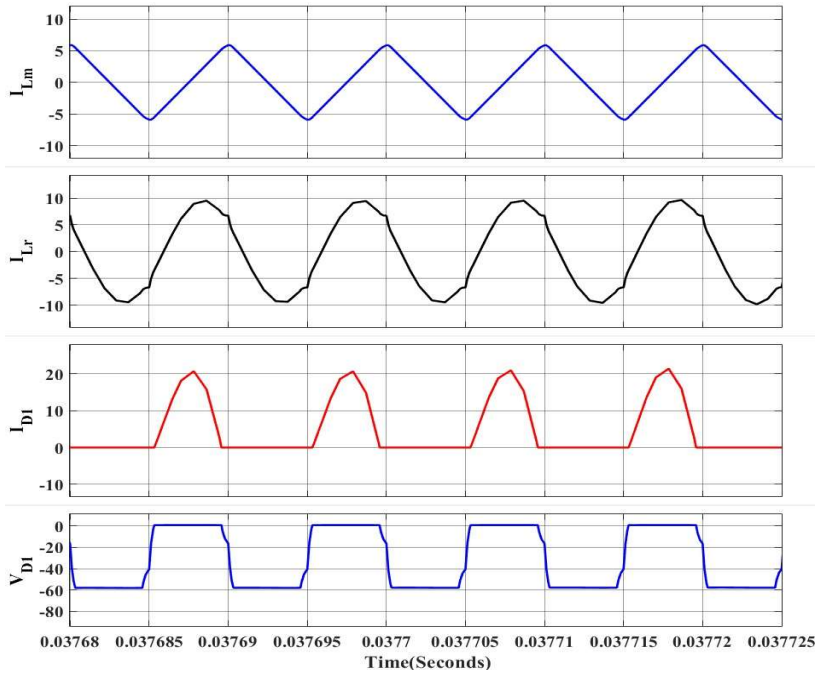

Fig. 4-14 Magnetization current, Resonance current, Diode current, and diode voltage in resonance mode

The magnetizing current and resonant current are depicted in Fig. 4-16. The resonant current and magnetizing current have an RMS value of 4.412 A, 2.534.A respectively. The resonant current is nearly sinusoidal in form, as can be shown in Fig. 4-16. The diode current and diode voltage are also in this fig. 4-16.

4.7.2 Boost mode of operation:

The simulation results for step-up mode (fs<fr) are shown using the switching frequency fs = 80kHz. As seen in Fig. 4-17, the predicted gain at 80kHz is 1.17.

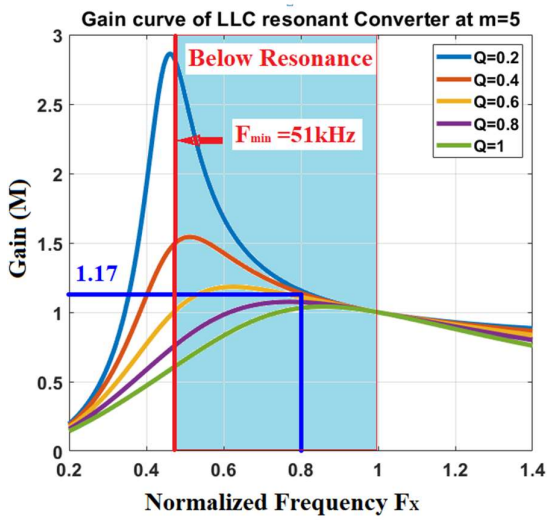

Fig.4-15 Boost mode operation

For the source voltage 420 V the output voltage is shown in Fig. 4-18 i.e. 68.3V.

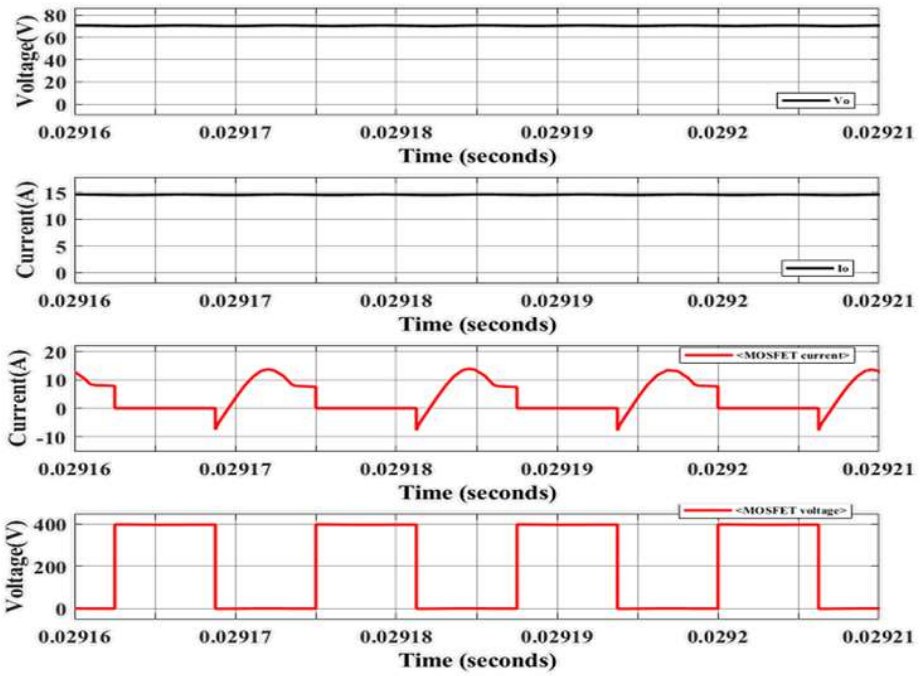

Fig. 4-16 Output Voltage, Output Current, Mosfet current and Voltage across MOSFET in Boost mode

The gain may be calculated using equation (7). The gain and ripple voltage are 1.168, and 0.35V respectively, which is larger than the ripple seen in resonance modes, with output voltages of 68.3V (upper limit) and 67.95V (lower limit). For this application, the simulation provided an output current of 13.70 A. The ripple current is 0.1 A, which is greater than the resonance mode ripple. Mosfet current is also shown in this fig. 4-19. the peak voltage across Q1 is 420 V, is displayed.

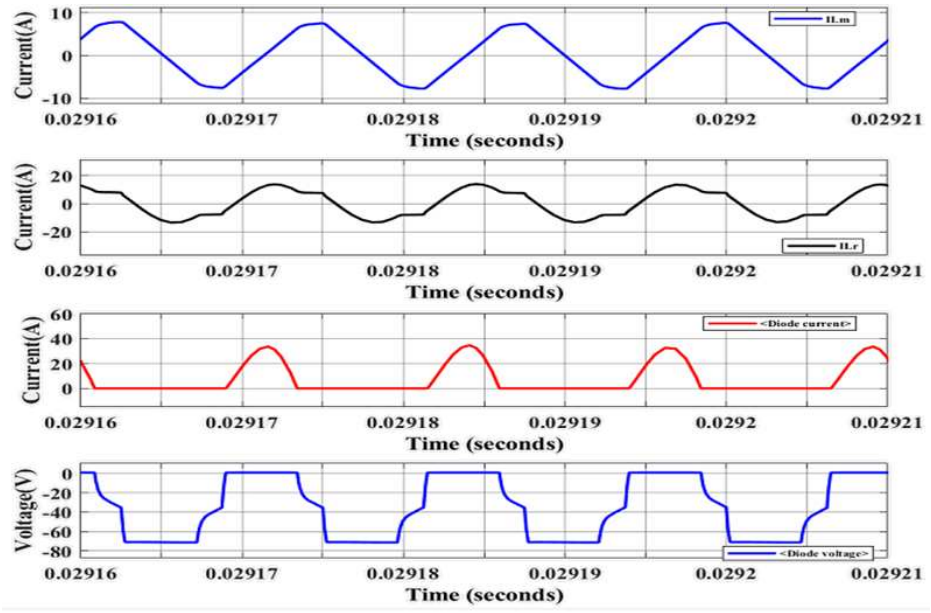

Fig.4-17 Magnetization current, Resonance Current, Diode current, and Diode voltage in Boost mode

In comparison to currents in resonance mode, the peak value of I_p and I_m is large, due to this primary coil conduction losses increases. In Fig. 4-22 the peak voltage across Q1 is 420 V.

4.7.3 Buck Mode of Operation

The DC-DC converter is simulated in Buck mode (fs>fr) with a switching frequency of 120kHz. As seen in Fig.4-20, the estimated gain is 0.88.

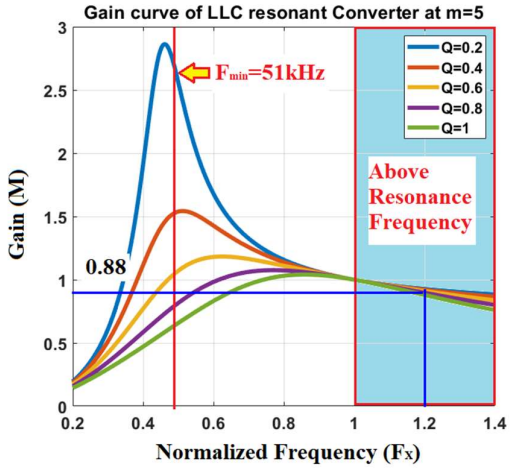

Fig.4-18 Buck mode operation

As shown in Fig. 4-21, the output voltage is 51.72V, with a ripple voltage of 0.1V. The peak point is 51.72V, while the low point is 51.62V. By using the equation (7) gain is 0.886.the output current is 10.70A with a current ripple of 0.05A at a frequency of 120kHz.

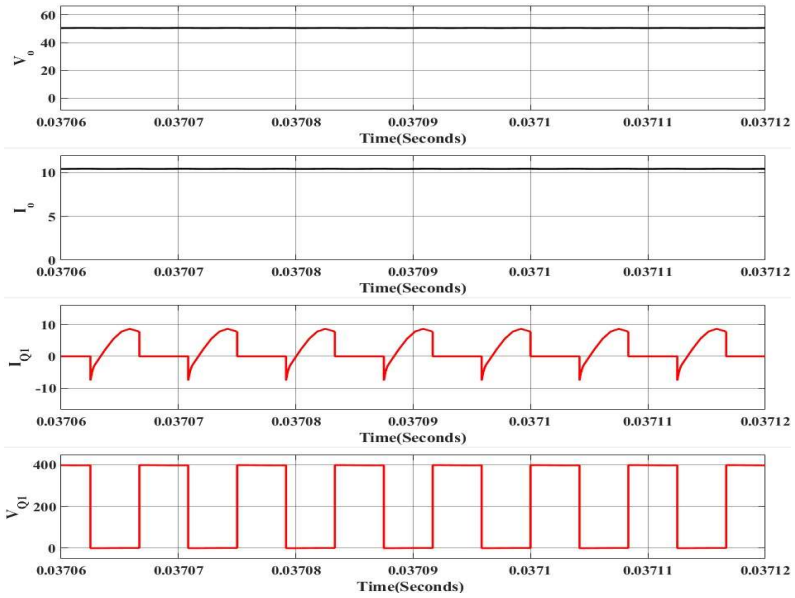

Fig. 4-19 Output Voltage, Output Current, Mosfet current, and Voltage across MOSFET in Buck mode

Mosfet current is also shown in this fig. 4-21. The value of Vd is 420 V, and ZVS is accomplished.

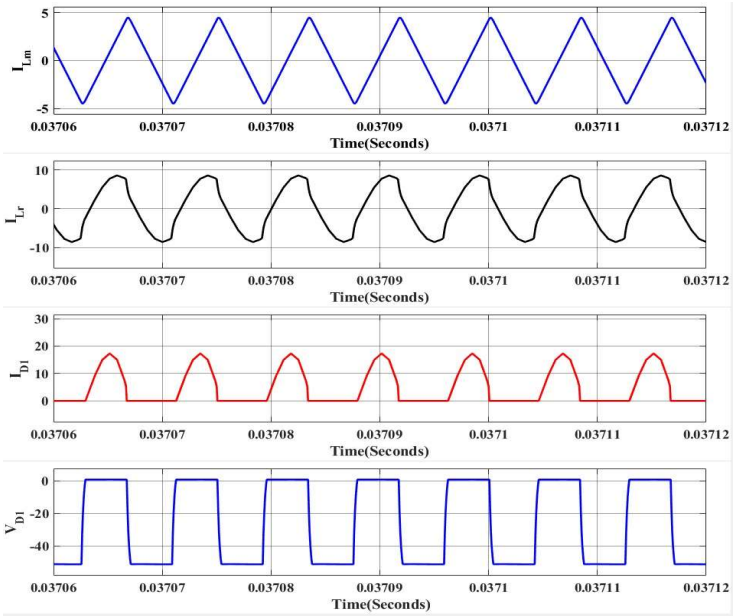

Fig.4-20 Magnetization current, Resonance Current, Diode current and Diode voltage in Buck mode

The resonance current (Ip) has an RMS value of 4.05 A, whereas the magnetizing current (Im) has an RMS value of 1.833A.

As a result, the resonance mode has the greatest result across all three modes of operation. It has been determined that charging the battery at a frequency close to the resonance frequency is the best approach.

4.7.4 LLC resonant converter performance

The steady-state performance of the Half-Bridge LLC resonant converter is discussed here. The battery voltage V_o = 48V is achieved with load current I_o = 12A. The peak amplitude of magnetizing current I_{Lm} is 1.2A shown in fig.5-6. with triangular current waveform and resonant current I_{Lr} has a peak value of 5.1A. The voltage across the capacitor V_{Cr} has a maximum value of 404V for the load P_o =576 W. The rectifier output current I_d is in continuous current mode with a peak amplitude of 21A.

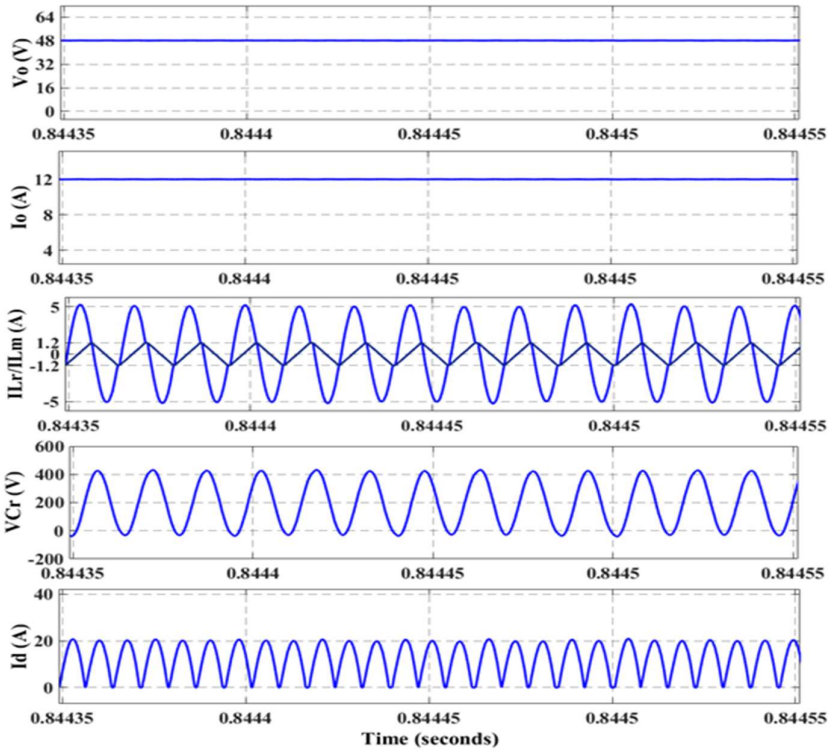

Fig. 4-21 Performance of battery voltage (V_o), battery current (I_o), resonant current (I_{Lr}), magnetizing current (I_{Lm}), resonant capacitor voltage (V_{Cr}), and rectifier current (I_d) at load (P_o)=576 W.

Power Factor variation under different Input voltages

The proposed battery charger is tested under various AC mains supply voltage range from 150V to 260V and a maximum Total Harmonic Distortion (THD) 3.18% is observed at a high input voltage 260V with power factor PF = 0.99949 for the load P_o =576W.

Table 4.1 Power Factor at different Supply Voltages

V_s (V)	I_s (A)	PF	THD (%)	P_o (W)
150	4.129	0.99962	2.75	576
160	3.877	0.99966	2.61	576
170	3.643	0.99969	2.48	576
180	3.441	0.99969	2.49	576
190	3.260	0.99971	2.39	576
200	3.097	0.99966	2.60	576
210	2.949	0.99968	2.52	576
220	2.815	0.99965	2.63	576
230	2.693	0.99964	2.70	576
240	2.581	0.99958	2.89	576
250	2.477	0.99953	3.07	576
260	2.382	0.99949	3.18	576

Table 4.2 Efficiency data:

Input voltage	Output Power (% of 250W)				
	20%	40%	60%	80%	100%
36V	97.1%	97.1%	97.1%	97.1%	97.1%
33V	96%	97.2%	97.6%	97.6%	97.4%
24V	94.5%	96.8%	97.1%	97.0%	
18V	94%	96.3%	96.2%		

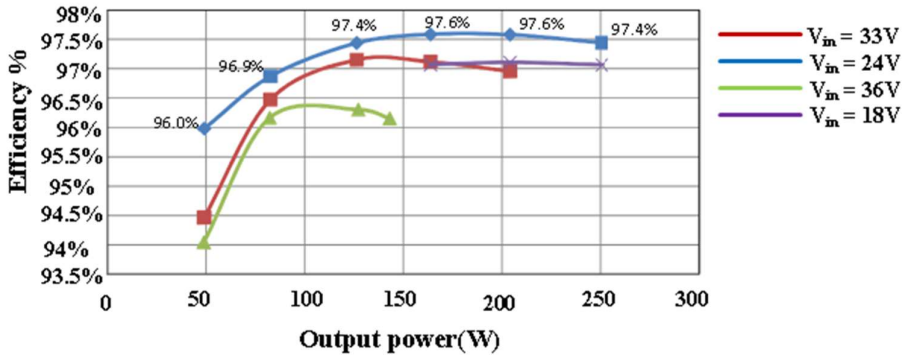

Fig.4.22 Efficiency of converter for changing power output for various input voltages.

Figure 4-23 depicts the converter's efficiency fluctuation for max and min input voltages at various output powers and a constant output voltage of 58V. Efficiency is 96.3 % for output power of 700W is achieved at a supply voltage of 420 V. At 340V supply voltage, efficiency is 96% for output power is achieved.

4.8 Conclusion

This chapter describes the basic operation of the half-bridge LLC resonance converter in resonant mode, step-down mode, and step-up mode. In this, we used the PI and PFM controller. PI is used for producing the control frequency spectrum. PFM controller converts the control frequency signal into a pulse. In this, we observed the ripple current, resonant peak current, magnetizing peak current, and ripple voltage in all three modes. By comparing currents in resonance mode, the peak current of resonant current and magnetizing current is largely due to this primary side conduction losses increase in boost mode. A power factor corrected Half-Bridge LLC resonant converter is designed for battery charging applications in electric vehicles. The proposed topology steady-state has been evaluated under load and supply voltage variations. For various input voltages, the power factor was evaluated. Smooth sinusoidal input current is shown to have excellent performance. In all three modes, the resonant mode provides excellent results. In this, we determined that charging the battery near the resonance frequency is the best to approach.

CHAPTER 5

CONCLUSION AND FUTURE SCOPE

5.1. CONCLUSION

A front-end AC-DC converters for PFC and DC-DC converters to manage the output side voltage and current are common components of an onboard Electric Vehicle battery charger system. Full-bridge DC-DC converters with isolated transformers and switches are widely utilized as the connection between the front-end converter and the EV battery to provide galvanic isolation, charging/discharging control, and flexibility of installation on Electric Vehicles. **Chapter 2**describes the literature survey. In this chapter discussed types of DC-DC converter i.e. buck, boost, buck-boost, flyback, sepic, cuk, voltage lift, Super lift, ultra-lift etc, Different types of electric vehicles i.e. hybrid EV, plug-in hybrid EV etc, types of battery i.e. Lithium-ion battery, Lead-acid battery etc, Battery charging of electric vehicles i.e. on-board and off-board battery charging, Soft-switching and LLC resonance converters. **Chapter 3** explained Power Factor Correction of the High Gain Luo Converter for EV Battery Charger with decreased system stresses. This deduction in switch voltage is produced in the conventional Luo converter by installing one switch and splitting the input inductor. While comparing the conventional Luo converter with the high gain Luo converter, For producing the same DC link voltage high gain Luo converter runs at a lower duty cycle due to the input switching inductor design, and lesser system stresses. This is suitable for high-power EV chargers since the switching voltage and current stresses are massively decreased. **Chapter 4** describes the basic operation of the half-bridge LLC resonance converter in resonant mode, step-down mode, and step-up mode. This chapter, used the PI and PFM controller. PI is used for producing the control frequency spectrum. PFM controller converts the control frequency signal into a pulse. This chapter observed the ripple current, resonant peak current, magnetizing peak current, and ripple voltage in all three modes. By comparing currents in resonance mode, the peak current of resonant current and magnetizing current is largely due to this primary side conduction losses increase in boost mode. A power factor corrected Half-Bridge LLC resonant converter is designed for battery charging applications in electric vehicles. The proposed topology

steady-state has been evaluated under load and supply voltage variations. For various input voltages, the power factor was evaluated. Smooth sinusoidal input current is shown to have excellent performance. In all three modes, the resonant mode provides excellent results. In this chapter, determined that charging the battery near the resonance frequency is the best to approach.

5.2. FUTURE SCOPE:

The following directions are recommended as suitable options for future exploration based on the research work detailed in the thesis:

- For better performance in terms of efficiency, voltage transfer gain, device stresses, and total harmonic distortions used the ultra-lift technique in the place of high gain Luo converter for battery charging.
- For control the battery voltage, battery current, and dc-link voltage of high gain Luo converter by Sliding mode controller (SMC), Fuzzy logic control (FLC), Adaptive Neuro-Fuzzy Inference System (ANFIS) controller, etc is used. For the future improvements, used digital control i.e. Digital signal processing (DSP). It can compute all the calculations in an only a single chip.
- Now come to the PFC of high gain Luo converter followed by LLC resonant converter battery charger of EVs, we can further improve by designing the four elements resonance tank i.e. LLCC resonant converter. This is the best way to optimize of a battery charger.

REFERENCES

[1]. R.W. Erickson and D. Maksimovic, Fundamentals of Power Electronics, Second Edition, Kluwer Academic/Plenum Publishers, New York, 2001.

[2]. M. Rashid and F. L. Luo, H. Ye, Digital power electronics and applications, Elsevier academic press (USA), 2005.

[3]. F.L. Luo, H. Ye, "Super-lift boost converters", *IET Power Electronics*, Vol 7, Iss.7, 2014.

[4]. S. Sivakumar, M.J. Sathik, P.S. Manoj and G.Sundararajan: "An assessment on the performance of DC/DC converters for renewable energy applications", *Renewable and Sustainable Energy Reviews*, Elsivier, 2016.

[5]. F. L. Luo, "Advance dc-dc converters", CRC Press, Boca Raton, FL, USA, 2004.

[6]. F. L. Luo, "Positive output Luo converters: voltage lift technique", *IEE proceedings Electric Power Applications*, VOL. 146, NO. 4, pp. 415 – 432, July 1999.

[7]. F. L. Luo, "Negative output Luo converters: voltage lift technique", *IEE proceedings Electric Power Applications*, VOL. 146, NO. 2, pp. 208 – 224, March 1999.

[8]. F. L. Luo and H. Ye, "Positive output super-lift converters", *IEEE Transactions on Power Electronics*, VOL. 18, NO. 1, pp. 105 – 113, January. 2003.

[9]. D. Liebal, P. Vijayraghavan, and N. Sreenath, "Control of dc-dc buck-boost converter using exact linearization techniques", *Power Electronics Specialists Conference, 1993. PESC '93 Record, 24th Annual IEEE*, pp. 203 – 207, 20-24 June 1993.

[10]. D.Cazrkowski, L. R. Pujara, and M. K. Kazimierzuk, "Robust stability of state-feedback control of PWM dc-dc push-pull converter", *IEEE Transactions on Industrial Electronics*, VOL. 42, NO. 1, pp. 108 – 111, February 1995.

[11]. M. K. Kazimierczuk and L. A. Starman, "Dynamic performance of PWM dc-dc boost converter with input voltage feedforward control", *IEEE*

Transactions on Circuits and Systems – I: Fundamental Theory and Applications, VOL. 46, NO. 12, pp. 1473 – 1481, December 1999.

[12]. H. Sira-Ramirez, "Nonlinear P-I controller design for switch mode dc-to-dc", pp. 410 – 417, April 1991.

[13]. K. Viswanathan, D. Srinivasan and R. Oruganti, "A universal fuzzy controller for a nonlinear power electronic converter", *in Proceedings of the 2002 IEEE International Conference on Fuzzy Systems*, VOL. 1, pp. 46 – 51, May 12-17 2002.

[14]. G. Perry, G. Feng, Y. F. Liu, and P. C. Sen, "A new sliding mode like control method for Buck converter", *in proceedings of 35th Annual IEEE Power Electronics Specialists Conference, PESC '2004*, VOL. 5, pp. 3688 – 3693, June 2004.

[15]. P. Mattavelli, L. Rosserro, G. Spiazzi and P. Tenti, "General-purpose fuzzy controller for dc-dc converters", *IEEE Transactions on Power Electronics*, VOL. 12, NO. 1, pp. 79 – 86, January 1997.

[16]. D. K. He and R. M. Nelms, "Peak current-mode control for a boost converter using an 8-bit microcontroller", *in proceedings of 34th IEEE Annual Power Electronics Specialist Conference, 2003. PESC '03*, VOL. 2, pp. 938 – 943, June 15-19 2003.

[17]. V. I. Uktin and A. Sabanovic, "Sliding modes applications in power electronics and motion control systems", *Proceedings of the IEEE International Symposium on Industrial Electronics, ISIE '99,* VOL. 1, pp. TU22 - TU31, 12-16 July 1999.

[18]. M. Oppenheimer, I. Husain, M. Elbuluk and J. A. De Abreu-Garcia, "Sliding mode control of the Cúk converter", *in proceedings of IEEE Power Electronics Specialists Conference*, *1996*. VOL. 2, pp. 1519 –1526, June 1996.

[19]. H. Sira-Ramirez, G. Escobar and R. Ortega, "On passivity-based sliding mode control of switched dc-to-dc power converters*", in proceedings of 35th Conference on Decision and Control,* TM17, pp. 2525 – 2526, December 1996.

[20]. S. P. Huang, H. Q. Xu, and Y. F. Liu, "Sliding-mode controlled Cúk switching regulator with fast response and first-order dynamic characteristic", *IEEE Power Nanyang Technological University Library Bibliography 189*

Electronics Specialists Conference, 1989, VOL. 1, pp. 124 – 129, 26-29 June 1989.

[21]. P. Mattavelli, L. Rossetto; G. Spiazzi and P. Tenti, “General-purpose sliding-mode controller for dc/dc converter applications”, *Power Electronics Specialists Conference, 1993. PESC '93 Record*, pp. 609 – 615, 20-24 June 1993.

[22]. E. Vidal-Idiarte, L. Martinez-Salamero, F. Guinjoan, J. Calvente and S. Gomariz, “Sliding and fuzzy controller of a Boost converter using an 8-bit microcontroller”, *in IEE proceedings on Electric Power Applications*, VOL. 151, NO. 1, pp. 5 – 11, January 2003.

[23]. J. C. Mukherjee and A. Gupta, "A Review of Charge Scheduling of Electric Vehicles in Smart Grid," *IEEE Systems Journal*, vol. 9, pp. 1541-1553, 2015.

[24]. C. C. Chan, "An overview of electric vehicle technology," *Proceedings of the IEEE*, vol. 81, pp. 1202-1213, 1993.

[25]. Z. Xiaohu, S. Lukic, S. Bhattacharya, and A. Huang, "Design and control of grid-connected converter in bi-directional battery charger for Plug-in hybrid electric vehicle application," *in Vehicle Power and Propulsion Conference, 2009. VPPC '09. IEEE*, pp. 1716-1721, 2009.

[26]. N. Daina and J. W. Polak, “Hazard based modeling of electric vehicles charging patterns,” *in Transportation Electrification Asia-Pacific (ITEC Asia-Pacific), 2016 IEEE Conference and Expo. IEEE*, pp. 479– 484, 2016.

[27]. S. Deilami, A. S. Masoum, P. S. Moses, and M. A. Masoum, “Real-time coordination of plug-in electric vehicle charging in smart grids to minimize power losses and improve voltage profile,” *IEEE Transactions on Smart Grid*, vol. 2, no. 3, pp. 456–467, 2011.

[28]. J. C. Mukherjee and A. Gupta, "A Review of Charge Scheduling of Electric Vehicles in Smart Grid," *IEEE Systems Journal*, vol. 9, pp. 1541-1553, 2015.

[29]. Z. Xiaohu, S. Lukic, S. Bhattacharya, and A. Huang, "Design and control of grid-connected converter in bi-directional battery charger for Plug-in hybrid electric vehicle application," *in Vehicle Power and Propulsion Conference, 2009. VPPC '09. IEEE*, pp. 1716-1721, 2009.

[30]. U. K. Madawala and D. J. Thrimawithana, "A Bidirectional Inductive Power Interface for Electric Vehicles in V2G Systems," *IEEE Transactions on Industrial Electronics,* vol. 58, pp. 4789-4796, 2011.

[31]. H. Liu, Z. Hu, Y. Song, and J. Lin, "Decentralized Vehicle-to-Grid Control for Primary Frequency Regulation Considering Charging Demands," *IEEE Transactions on Power Systems*, vol. 28, pp. 3480-3489, 2013.

[32]. Westgeest and L. Brett, "Improving safety and performance testing for EV batteries," *in 2013 World Electric Vehicle Symposium and Exhibition (EVS27)*, pp. 1-4, 2013.

[33]. P. A. Cassani and S. S. Williamson, "Significance of Battery Cell Equalization and Monitoring for Practical Commercialization of Plug-In Hybrid Electric Vehicles," *in 2009 Twenty-Fourth Annual IEEE Applied Power Electronics Conference and Exposition*, pp. 465-471, 2009.

[34]. P. Ramadass, B. Haran, R. White, and B. N. Popov, "Performance study of commercial LiCoO2 and spinel-based Li-ion cells," *Journal of Power Sources*, vol. 111, pp. 210-220, 9 Sept. 2002.

[35]. W. Renhart, C. Magele, and B. Schweighofer, "FEM-Based Thermal Analysis of NiMH Batteries for Hybrid Vehicles," *IEEE Transactions on Magnetics*, vol. 44, pp. 802-805, 2008.

[36]. Hoke, A. Brissette, K. Smith, A. Pratt, and D. Maksimovic, "Accounting for Lithium-Ion Battery Degradation in Electric Vehicle Charging Optimization," *IEEE Journal of Emerging and Selected Topics in Power Electronics*, vol. 2, pp. 691-700, 2014.

[37]. Khaligh and Z. Li, "Battery, Ultracapacitor, Fuel Cell, and Hybrid Energy Storage Systems for Electric, Hybrid Electric, Fuel Cell, and Plug-In Hybrid Electric Vehicles: State of the Art," *IEEE Transactions on Vehicular Technology*, vol. 59, pp. 2806-2814, 2010.

[38]. S. Dey, B. Ayalew, and P. Pisu, "Combined estimation of State-of-Charge and State-of-Health of Li-ion battery cells using SMO on an electrochemical model," *in 2014 13th International Workshop on Variable Structure Systems (VSS)*, pp. 1-6, 2014.

[39]. Y. Attia, A. Abdelrahman, M. Hamouda, and M. Youssef, "SiC devices performance overview in EV DC/DC converter: A case study in a Nissan Leaf," *in 2016 IEEE Transportation Electrification Conference and Expo, Asia-Pacific (ITEC Asia-Pacific)*, pp. 214-219, 2016.

[40]. W. Liangrong, L. Jianing, X. Guoqing, X. Kun, and S. Zhibin, "A novel battery charger for plugin hybrid electric vehicles," *in Information and*

Automation (ICIA), 2012 International Conference on, pp. 168-173, 2012.

[41]. Y. D. Lee and S. Y. Park, "Rapid charging strategy in the constant voltage mode for a high power Li-Ion battery," *in 2013 IEEE Energy Conversion Congress and Exposition*, pp. 4725-4731, 2013.

[42]. S. R. Osman, N. A. Rahim, and S. Jeyraj, "Single current sensor with multiple constant current charging methods in solar battery charger," *in 3rd IET International Conference on Clean Energy and Technology (CEAT) 2014*, pp. 1-5, 2014.

[43]. M. Chen and G. A. Rincon-Mora, "Accurate, Compact, and Power-Efficient Li-Ion Battery Charger Circuit," *IEEE Transactions on Circuits and Systems II: Express Briefs*, vol. 53, pp. 1180- 1184, 2006

[44]. L. Yi-Hwa, T. Jen-Hao, and L. Yu-Chung, "Search for an optimal rapid charging pattern for lithium-ion batteries using ant colony system algorithm," *IEEE Transactions on Industrial Electronics*, vol. 52, pp. 1328-1336, 2005.

[45]. T. Kang, C. Kim, Y. Suh, H. Park, B. Kang, and D. Kim, "A design and control of bi-directional non-isolated DC-DC converter for the rapid electric vehicle charging system," *in 2012 IEEE International Conference on Information and Automation*, pp. 14-21, 2012.

[46]. J. G. Pinto, V. Monteiro, H. Gonçalves, and J. L. Afonso, "Onboard Reconfigurable Battery Charger for Electric Vehicles With Traction-to-Auxiliary Mode," *IEEE Transactions on Vehicular Technology*, vol. 63, pp. 1104-1116, 2014.

[47]. G. Y. Choe, J. S. Kim, B. K. Lee, W. Chung-Yuen, and L. Tea-Won, "A Bi-directional battery charger for electric vehicles using photovoltaic PCS systems," *in 2010 IEEE Vehicle Power and Propulsion Conference*, pp. 1-6, 2010.

[48]. E. Sortomme and M. A. El-Sharkawi, "Optimal Charging Strategies for Unidirectional Vehicleto-Grid," *IEEE Transactions on Smart Grid*, vol. 2, pp. 131-138, 2011.

[49]. W. Su, H. Eichi, W. Zeng, and M. Y. Chow, "A Survey on the Electrification of Transportation in a Smart Grid Environment," *IEEE Transactions on Industrial Informatics*, vol. 8, pp. 1-10, 2012.

[50]. E. Inoa and J. Wang, "PHEV Charging Strategies for Maximized Energy Saving," *IEEE Transactions on Vehicular Technology*, vol. 60, pp. 2978-

2986, 2011.

[51]. J. Gallardo-Lozano, M. I. Milanés-Montero, M. A. Guerrero-Martínez, and E. Romero-Cadaval, "Three-phase bidirectional battery charger for smart electric vehicles," *in 2011 7th International Conference-Workshop Compatibility and Power Electronics (CPE)*, pp. 371-376, 2011.

[52]. S. Y. Kim, H. S. Song, and K. Nam, "Idling Port Isolation Control of Three-Port Bidirectional Converter for EVs," *IEEE Transactions on Power Electronics*, vol. 27, pp. 2495-2506, 2012.

[53]. S. Pala and S. P. Singh, "Design, modeling and implementation of Bi-directional buck and boost converter," *in 2012 IEEE 5th India International Conference on Power Electronics (IICPE)*, pp. 1-6, 2012.

[54]. G. Hua and F. C. Lee, "Soft-switching techniques in PWM converters," *IEEE Transactions on Industrial Electronics*, vol. 42, pp. 595-603, 1995.

[55]. G. Y, L. Z, H. L, Q. Z, and H. G, "Three-level LLC series resonant DC/DC converter," *IEEE Transactions on Power Electronics*, vol. 20, pp. 781-789, 2005.

[56]. W. Chen, P. Rong, and Z. Lu, "Snubberless Bidirectional DC-DC Converter With New CLLC Resonant Tank Featuring Minimized Switching Loss," *IEEE Transactions on Industrial Electronics*, vol. 57, pp. 3075-3086, 2010.

[57]. Yang, F. C. Lee, A. J. Zhang, and H. Guisong, "LLC resonant converter for front end DC/DC conversion," *in Applied Power Electronics Conference and Exposition, 2002. APEC 2002. Seventeenth Annual IEEE*, pp. 1108-1112 vol.2, 2002.

[58]. Gould, C. M. Bingham, D. A. Stone, and M. P. Foster, "CLL resonant converters with output short-circuit protection," *Electric Power Applications, IEE Proceedings - 2005*, vol. 152, pp. 1296-1306, 2005.

[59]. H. Chang, C. Hung-Liang, C. En-Chih, C. Chun-An, and C. Hung-Yi, "Modeling and design of the LLC resonant converter used in solar array simulator," *in 2012 7th IEEE Conference on Industrial Electronics and Applications (ICIEA)*, pp. 653-658, 2012.

[60]. G. Pledl, M. Tauer, and D. Buecherl, "Theory of operation, design procedure and simulation of a bidirectional LLC resonant converter for vehicular applications," *IEEE Vehicle Power and Propulsion Conference*, 2010, pp. 1-5, 2010.